

The CORALIE survey for southern extrasolar planets. XVIII. Three new massive planets and two low-mass brown dwarfs at greater than 5 AU separation

E. L. Rickman, D. Ségransan, M. Marmier, S. Udry, F. Bouchy, C. Lovis, M. Mayor, F. Pepe, D. Queloz, N. C. Santos, et al.

▶ **To cite this version:**

E. L. Rickman, D. Ségransan, M. Marmier, S. Udry, F. Bouchy, et al.. The CORALIE survey for southern extrasolar planets. XVIII. Three new massive planets and two low-mass brown dwarfs at greater than 5 AU separation. Astronomy and Astrophysics - A&A, 2019, 625, 10.1051/0004-6361/201935356 . insu-03666752

HAL Id: insu-03666752
https://insu.hal.science/insu-03666752

Submitted on 13 May 2022

HAL is a multi-disciplinary open access archive for the deposit and dissemination of scientific research documents, whether they are published or not. The documents may come from teaching and research institutions in France or abroad, or from public or private research centers.

L'archive ouverte pluridisciplinaire **HAL**, est destinée au dépôt et à la diffusion de documents scientifiques de niveau recherche, publiés ou non, émanant des établissements d'enseignement et de recherche français ou étrangers, des laboratoires publics ou privés.

A&A 625, A71 (2019)
https://doi.org/10.1051/0004-6361/201935356
© ESO 2019

Astronomy & Astrophysics

The CORALIE survey for southern extrasolar planets

XVIII. Three new massive planets and two low-mass brown dwarfs at greater than 5 AU separation★,★★

E. L. Rickman[1], D. Ségransan[1], M. Marmier[1], S. Udry[1], F. Bouchy[1], C. Lovis[1], M. Mayor[1], F. Pepe[1], D. Queloz[1], N. C. Santos[2,3], R. Allart[1], V. Bonvin[4], P. Bratschi[1], F. Cersullo[1], B. Chazelas[1], A. Choplin[1], U. Conod[1], A. Deline[1], J.-B. Delisle[1], L. A. Dos Santos[1], P. Figueira[5,2], H. A. C. Giles[1], M. Girard[1], B. Lavie[1], D. Martin[1,★★★,6], F. Motalebi[1], L. D. Nielsen[1], H. Osborn[7,8], G. Ottoni[1], M. Raimbault[1], J. Rey[1,9], T. Roger[1,10], J. V. Seidel[1], M. Stalport[1], A. Suárez Mascareño[1,11], A. Triaud[12], O. Turner[1], L. Weber[1], and A. Wyttenbach[1,13]

(Affiliations can be found after the references)

Received 25 February 2019 / Accepted 2 April 2019

ABSTRACT

Context. Since 1998, a planet-search around main sequence stars within 50 pc in the southern hemisphere has been underway with the CORALIE spectrograph at La Silla Observatory.
Aims. With an observing time span of more than 20 yr, the CORALIE survey is able to detect long-term trends in data with masses and separations large enough to select ideal targets for direct imaging. Detecting these giant companion candidates will allow us to start bridging the gap between radial-velocity-detected exoplanets and directly imaged planets and brown dwarfs.
Methods. Long-term precise Doppler measurements with the CORALIE spectrograph reveal radial-velocity signatures of massive planetary companions and brown dwarfs on long-period orbits.
Results. In this paper, we report the discovery of new companions orbiting HD 181234, HD 13724, HD 25015, HD 92987 and HD 50499. We also report updated orbital parameters for HD 50499b, HD 92788b and HD 98649b. In addition, we confirm the recent detection of HD 92788c. The newly reported companions span a period range of 15.6–40.4 yr and a mass domain of 2.93–26.77 $M_{\rm Jup}$, the latter of which straddles the nominal boundary between planets and brown dwarfs.
Conclusions. We report the detection of five new companions and updated parameters of four known extrasolar planets. We identify at least some of these companions to be promising candidates for imaging and further characterisation.

Key words. techniques: radial velocities – planets and satellites: detection – binaries: visual – planetary systems

1. Introduction

Little is known about massive giant planets and brown dwarfs at orbital separations between 5 and 50 AU due to their low occurrence rate (Bowler 2016) and to the lower sensitivity of the different observing methods in this separation range. Indeed, radial velocity (RV) and transit techniques are extremely efficient at detecting planets around older stars at short separations (Fischer et al. 2014). On the other hand, direct imaging is most efficient at detecting younger planets at separations larger than several times the diffraction limit of the telescope (typically 5–10 λ/D). This translates into several tens of astronomical units for the closest young stellar associations (e.g. β Pic and 51 Eri as part of the β Pic moving group (Zuckerman et al. 2001; Feigelson et al. 2006) and HR 8799 as part of the Columba association (Zuckerman et al. 2011). Nevertheless, the population of massive giant exoplanets at intermediate orbital separations between 5 and 50 AU is an important puzzle piece needed for constraining the uncertainties that exist in planet formation and evolution models.

The historical CORALIE planet-search survey has been ongoing for more than 20 yr in the southern hemisphere and monitors a volume-limited sample of 1647 main sequence (MS) stars from F8 down to K0 located within 50 pc of the Sun (Udry et al. 2000). With an individual measurement precision ranging between 3.5 and 6 ms^{-1}, CORALIE has permitted (or has contributed to) the detection of more than 140 extra-solar planet candidates (Pepe et al. 2002; Udry et al. 2002; Tamuz et al. 2008; Ségransan et al. 2010; Marmier et al. 2013). Such a long and continuous monitoring of nearby MS stars is unique among all planet search surveys; it allows us to detect massive giant planets at separations larger 5 AU as well as to identify small RV drifts

★ The radial velocity measurements and additional data products discussed in this paper are available on the DACE web platform at https://dace.unige.ch/radialVelocities. See the appendix for a direct link to the individual target data products. A copy of the data is also available at the CDS via anonymous ftp to cdsarc.u-strasbg.fr (130.79.128.5) or via http://cdsarc.u-strasbg.fr/viz-bin/qcat?J/A+A/625/A71

★★ Based on observations collected with the CORALIE spectrograph mounted on the 1.2 m Swiss telescope at La Silla Observatory and with the HARPS spectrograph on the ESO 3.6 m telescope at La Silla (ESO, Chile).

★★★ Fellow of the Swiss National Science Foundation.

hinting at the presence of low-mass companions at even wider separations.

These are indeed very useful targets for direct imaging, as such old and very-low-mass companions are rare and very difficult to search for blindly. Cheetham et al. (2018) has shown with the discovery of the ultra-cool brown dwarf companion orbiting the planet host star HD 4113 A that long-term RV surveys are an extremely useful tool to select targets to image. Not only does it allow us to start filling in a largely unexplored parameter space, but through combining RV and direct imaging we can now expect to measure the masses of these companions using Kepler's laws. By constraining the mass, we are able to place additional constraints on the evolution of the companion, both in terms of temperature and atmospheric composition (Crepp et al. 2018; Peretti et al. 2019).

In this paper we report the discovery of four new giant planets and brown dwarfs orbiting HD 181234, HD 13724, HD 25015, and HD 92987, together with the updated CORALIE orbital elements for an already known exoplanet around HD 98649 (Marmier et al. 2013). We also report updated orbital parameters for HD 50499b (Vogt et al. 2005), as well as the detection of HD 50499c, which has previously been noted by Vogt et al. (2005), Butler et al. (2017), and Barbato et al. (2018). We also report the updated orbital parameters of HD 92788b detected by Fischer et al. (2001) and confirm the recent detection of HD 92788c (Wittenmyer et al. 2019).

The paper is organised as follows. The properties of the host stars are summarised in Sect. 2. In Sect. 3 we present our RV data and the inferred orbital solution of the newly detected companions. In Sect. 4 we present the CORALIE updated parameters of already known exoplanets with new detections in two of these systems. The results are discussed in Sect. 5 with some concluding remarks.

2. Stellar characteristics

Spectral types, V band magnitude and colour indices are taken from the HIPPARCOS catalogue (Perryman et al. 1997) while astrometric parallaxes (π) and luminosities are taken from the second *Gaia* date release (Gaia Collaboration 2018). Effective temperatures, gravities, and metallicities are derived using the same spectroscopic methods as applied in Santos et al. (2013), whilst the $v \sin(i)$ is computed using the calibration of CORALIE's cross correlation function (CCF; Santos et al. 2001; Marmier 2014).

The mean chromospheric activity index – $\log(R'_{\rm HK})$ – of each star is computed by co-adding the corresponding CORALIE spectra to improve the signal-to-noise ratio (S/N) which allows us to measure the Ca II re-emission at λ = 3933.66 Å. We derived an estimate of the rotational period of the star from the mean $\log(R'_{\rm HK})$ activity index using the calibration of Mamajek & Hillenbrand (2008).

Stellar radii and their uncertainties are derived from the *Gaia* luminosities and the effective temperatures obtained from the spectroscopic analysis. A systematic error of 50 K was quadratically added to the effective temperature error bars and was propagated in the radius uncertainties.

The mass and the age of the stars, as well as their uncertainties, are derived using the Geneva stellar-evolution models (Ekström et al. 2012; Georgy et al. 2013). The interpolation in the model grid was made through a Bayesian formalism using observational Gaussian priors on $T_{\rm eff}$, $M_{\rm V}$, $\log g$, and [Fe/H] (Marmier 2014).

The observed and inferred stellar parameters for newly detected host stars to planetary companions are summarised in Table 1 and host stars to brown dwarf companions in Table 2.

3. Radial velocities and orbital solutions

The CORALIE observations span over more than 20 yr, from June 1998 to December 2018. During that time, CORALIE went through two major upgrades in June 2007 (Ségransan et al. 2010) and in November 2014 to increase overall efficiency and accuracy of the instrument. These changes introduced small offsets in the measured RVs that depend on several parameters such as the spectral type of the star and its systemic velocity. For this reason, we decided to consider CORALIE as three different instruments, corresponding to the different upgrades: the original CORALIE as CORALIE-98 (C98), the first upgrade as CORALIE-07 (C07), and the latest upgrade as CORALIE-14 (C14).

In addition to the RV time series, the CORALIE automated pipeline also provides several useful indicators that help pinpoint the origin of observed periodic signals. These are the CCF full width at half maximum (FWHM), the bisector, and the H_α chromospheric activity indicator.

We are also using published RVs taken with other spectrographs, namely HARPS (Mayor et al. 2003), HIRES (Vogt et al. 1994), and HAMILTON (Vogt 1987). The data products presented in this paper are available at the Data and Analysis Center for Exoplanets (DACE)[1].

We perform an initial modelling of the RV time series using the online DACE platform. Keplerian model initial conditions are computed using the formalism described in Delisle et al. (2016). The stellar activity detrending and the modelling of the instrumental noise and the stellar jitter follow the formalism described in Díaz et al. (2016) and Delisle et al. (2018). Analytical false-alarm probabilities (FAPs) are computed on the periodogram of the residuals following Baluev (2008) and numerical FAP values which are used in this paper are computed by permutation of the calendar. Periodic signals with a FAP lower than 0.1% are considered significant and are added to the model. For each periodogram shown, the three lines represent the 10, 1, and 0.1% FAP in ascending order.

Once the RV time series is fully modelled using DACE online tools, we run a Markov chain Monte Carlo (MCMC) analysis of each system using the algorithm described in Díaz et al. (2014, 2016) and Delisle et al. (2018) to obtain the posterior distributions of the model parameters. Each MCMC simulation is run with 10 000 000 iterations drawing the proposal solution obtained using DACE. The parameter confidence intervals are computed for a 68.27% confidence level.

Gaussian priors are set for the instrument offsets and stellar mass with uniform priors for the orbital elements. In the cases where the minimum RV ($T_{V_{\rm min}}$) or the maximum RV ($T_{V_{\rm max}}$) is well sampled, we perform the fit using either of these instead of fitting the phase.

In this section we present the orbital solutions for newly reported giant planets and brown dwarfs from the CORALIE survey. A summary of the orbital solutions can be found in Table 3 for the newly detected companions and the fully probed MCMC parameter space is shown in the appendix.

[1] The data are available at the Data and Analysis Center for Exoplanets (DACE) which can be accessed at https://dace.unige.ch

Table 1. Observed and inferred stellar parameters for host stars to the planet candidates: HD 181234, HD 25015, HD 50499, HD 92788, and HD 98649.

Parameters	Units	HD 181234	HD 25015	HD 50499	HD 92788	HD 98649
Spectral type [a]		G5	K1V	G1V	G6V	G3/G5V
V [a]		8.59	8.87	7.21	7.31	8.00
$B-V$ [a]		0.841	0.899	0.614	0.694	0.658
π [b]	(mas)	20.9 ± 0.06	26.7 ± 0.05	21.58 ± 0.03	28.83 ± 0.05	23.7 ± 0.05
L [b]	($L_\odot$)	0.80 ± 0.003	0.41 ± 0.001	2.38 ± 0.005	1.25 ± 0.003	0.98 ± 0.003
$T_{\rm eff}$ [c]	(K)	5386 ± 60	5160 ± 63	6099 ± 43	5744 ± 24 [e]	5790 ± 58
$\log g$ [c]	(cgs)	4.25 ± 0.11	4.40 ± 0.14	4.42 ± 0.05	4.39 ± 0.04	4.51 ± 0.09
[Fe/H] [c]	(dex)	0.32 ± 0.05	0.04 ± 0.04	0.38 ± 0.03	0.27 ± 0.02 [e]	0.05 ± 0.04
$\log R'_{\rm HK}$ [c]		−5.17 ± 0.01	−4.48 ± 0.002	−5.08 ± 0.004	−4.98 ± 0.01 [f]	−5.06 ± 0.005
$P_{\rm rot}$	(days)	50.8 ± 2.0	13.6 ± 2.3	22.4 ± 1.0	31.0 ± 1.4 [g]	27.7 ± 1.2
$v \sin i$ [d]	(km s^{-1})	2.105	3.485	4.313	2.719	2.218
M_*	($M_\odot$)	1.01 ± 0.06	0.86 ± 0.05	1.31 ± 0.07	1.15 ± 0.07	1.03 ± 0.06
R_*	($R_\odot$)	1.05 ± 0.07	0.83 ± 0.04	1.42 ± 0.02	1.14 ± 0.02	1.01 ± 0.02
Age	(Gyr)	6.32 ± 2.58	4.00 ± 3.41	2.40 ± 0.56	2.55 ± 1.51	2.42 ± 1.62

Notes. [a] Parameters taken from HIPPARCOS (Perryman et al. 1997). [b]Parameters taken from *Gaia* data release 2 (Gaia Collaboration 2018). [c]Parameters derived using CORALIE spectra. [d]Parameters derived using CORALIE CCF. [e]Parameters taken from Sousa et al. (2008). [f]Parameters derived using HARPS spectra. [g]From the calibration of the rotational period vs. activity (Mamajek & Hillenbrand 2008).
Refrences. (1) Gaia Collaboration (2018); (2) Mamajek & Hillenbrand (2008); (3) Perryman et al. (1997); (4) Sousa et al. (2008).

Table 2. Observed and inferred stellar parameters for host stars to the brown dwarf candidates: HD 13724 and HD 92987.

Parameters	Units	HD 13724	HD 92987
Spectral type [a]		G3/G5V	G2/G3V
V [a]		7.89	7.03
$B-V$ [a]		0.667	0.641
π [b]	(mas)	23.0 ± 0.03	22.9 ± 0.03
L [b]	($L_\odot$)	$1.14^{+0.001}_{-0.002}$	2.55 ± 0.006
$T_{\rm eff}$ [c]	(K)	5868 ± 27 [e]	5770 ± 36 [f]
$\log g$ [c]	(cgs)	4.44 ± 0.07 [g]	4.00 ± 0.15 [f]
[Fe/H] [c]	(dex)	0.23 ± 0.02 [e]	−0.08 ± 0.08 [f]
$\log R'_{\rm HK}$ [c]		−4.76 ± .003	−5.090 ± 0.006
$P_{\rm rot}$	(days)	20.2 ± 1.2	26.2 ± 1.1
$v \sin i$ [d]	(km s^{-1})	3.025	2.616
M_*	($M_\odot$)	1.14 ± 0.06	1.08 ± 0.06
R_*	($R_\odot$)	1.07 ± 0.02	1.58 ± 0.04
Age	(Gyr)	0.76 ± 0.71	7.75 ± 0.31

Notes. [a]Parameters taken from HIPPARCOS (Perryman et al. 1997). [b]Parameters taken from *Gaia* data release 2 (Gaia Collaboration 2018). [c]Parameters derived using CORALIE spectra. [d]Parameters derived using CORALIE CCF. [e]Parameters taken from Gomes da Silva et al. (2014). [f]Parameters taken from Bond et al. (2006). [g]Parameters taken from Porto de Mello et al. (2014).
References. (1) Bond et al. (2006); ; (2) Gaia Collaboration (2018); (3) Gomes da Silva et al. (2014); (4) Perryman et al. (1997); (5) Porto de Mello et al. (2014).

3.1. HD 181234 (LTT 5654, HIP 95015)

HD 181234 was observed with CORALIE at La Silla Observatory since May 2000. Fifteen measurements were taken with CORALIE-98, 21 additional RV measurements were obtained with CORALIE-07, and 59 additional RV measurements were obtained with CORALIE-14. HD 181234 has also been observed with Keck/HIRES (Butler et al. 2017) with 20 RV measurements from June 1999 to August 2014.

The best-fit Keplerian, as shown in Fig. 1, shows that we are looking at a highly eccentric system with an eccentricity of 0.73. It has an orbital period of 20.4 yr with a minimum mass of 8.4 $M_{\rm Jup}$. The orbital solutions are summarised in Table 3. Figure 1 shows the CORALIE RVs and the corresponding best-fit Keplerian model along with the RV residuals and a periodogram of the residuals. The results from the fully probed parameter space from the MCMC are shown in the appendix.

3.2. HD 92987 (HIP 52472)

HD 92987 was observed with CORALIE at La Silla Observatory since January 1999. Fifty-three measurements were taken with CORALIE-98, 18 additional RV measurements were obtained with CORALIE-07, and 22 additional RV measurements were obtained with CORALIE-14.

HD 92987b is one of the brown dwarf candidates with a minimum mass of 16.88 $M_{\rm Jup}$ and a semi-major axis of 9.62 AU, making it a promising candidate for direct imaging. The orbital solutions for HD 92987 are summarised in Table 3. Figure 2 shows the CORALIE RVs and the corresponding best-fit Keplerian model along with the RV residuals and a periodogram of the residuals. The results from the fully probed parameter space from the MCMC are shown in the appendix.

3.3. HD 25015 (HIP 18527)

HD 25015 was observed with CORALIE at La Silla Observatory since May 2001. Twenty-two measurements were taken with CORALIE-98, 32 additional RV measurements were obtained with CORALIE-07, followed by 56 additional RV measurements obtained with CORALIE-14.

Table 3. Best-fitted solutions for the substellar companions orbiting HD 13724, HD 181234, HD 25015, and HD 92987.

Parameters	Units	HD 13724b	HD 181234b	HD 25015b	HD 92987b
P	(yr)	$40.42^{+13.42}_{-4.38}$	$20.43^{+0.22}_{-0.21}$	$16.48^{+1.86}_{-0.72}$	$28.35^{+1.51}_{-0.74}$
K	(ms^{-1})	$214.3^{+21.5}_{-10.2}$	$126.8^{+1.8}_{-1.6}$	$60.1^{+3.1}_{-3.2}$	$152.7^{+2.3}_{-2.7}$
e		$0.34^{+0.09}_{-0.05}$	0.73 ± 0.01	$0.39^{+0.09}_{-0.07}$	$0.21^{+0.02}_{-0.01}$
ω	(deg)	$187.5^{+2.9}_{-1.7}$	$93.3^{+1.7}_{-1.8}$	$77.7^{+9.8}_{-8.6}$	$195.1^{+6.7}_{-8.4}$
T_p	(JD)	6189.1^{+73}_{-54}	$7668.7^{+5.5}_{-5.0}$	5852^{+160}_{-140}	7889^{+130}_{-180}
$M. \sin i$	(M_{Jup})	$26.77^{+4.4}_{-2.2}$	$8.37^{+0.34}_{-0.36}$	$4.48^{+0.30}_{-0.28}$	$16.88^{+0.69}_{-0.65}$
a	(AU)	$12.40^{+2.6}_{-0.9}$	$7.52^{+0.16}_{-0.16}$	$6.19^{+0.45}_{-0.23}$	$9.62^{+0.36}_{-0.26}$
N_{RV}		167	115	110	93
ΔT	(yr)	19.3	18.6	17.6	19.9

Notes. For each parameter, the mode of the posterior is considered, with error bars computed from the MCMC chains with 10 000 000 iterations using a 68.27% confidence interval. ΔT is the time interval between the first and last measurements. C98 stands for CORALIE-98, C07 for CORALIE-07 and C14 for CORALIE-14. N_{RV} is the number of RV measurements. T_P is shown in BJD-2 450 000.

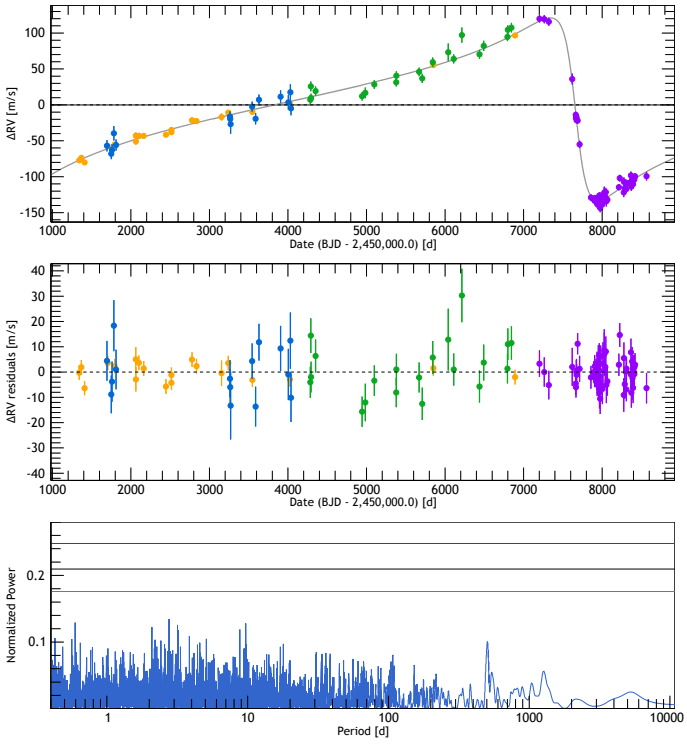


Fig. 1. *Top*: HD 181234 RV measurements as a function of Julian Date obtained with CORALIE-98 (blue), CORALIE-07 (green), CORALIE-14 (purple) and HIRES data (Butler et al. 2017) in orange. The best single-planet Keplerian model is represented as a black curve. *Middle*: RV residuals of HD 181234. *Bottom*: periodogram of the residuals for HD 181234. The three black lines represent the 10, 1, and 0.1% FAPs in ascending order.

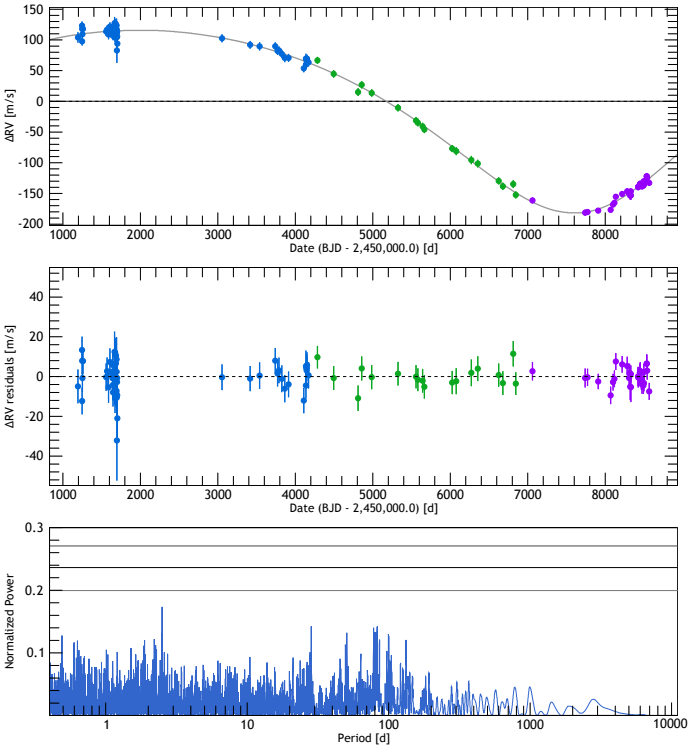


Fig. 2. *Top*: HD 92987 RV measurements as a function of Julian Date obtained with CORALIE-98 (blue), CORALIE-07 (green) and CORALIE-14 (purple). The fitted single-planet Keplerian model is represented as a black curve. *Middle*: RV residuals of HD 92987. *Bottom*: periodogram of the residuals for HD 92987. The three black lines represent the 10, 1 and 0.1% FAPs in ascending order.

We note here that all of the stars in our sample are very quiet with the exception of HD 25015. When we plot the H_α versus time, we see that some periodicity exists in the periodogram at a FAP of greater than 10%, as seen in Fig 3 at approximately 370.26 days. We do not see a periodicity in the FWHM or bisector, therefore we cannot exclude that there is telluric line contamination in the H_α index with CORALIE. We detrend the RV from the stellar activity using the H_α indicators. A scale factor is adjusted to the smoothed H_α (using a Gaussian filter at 0.1 yr), as well as an additional jitter term proportional to the activity trend.

The orbital solutions for HD 25015 are summarised in Table 3. Figure 3 shows the CORALIE RVs and the corresponding best-fit Keplerian model along with the RV residuals, the periodogram of the residuals and a periodogram for H_α

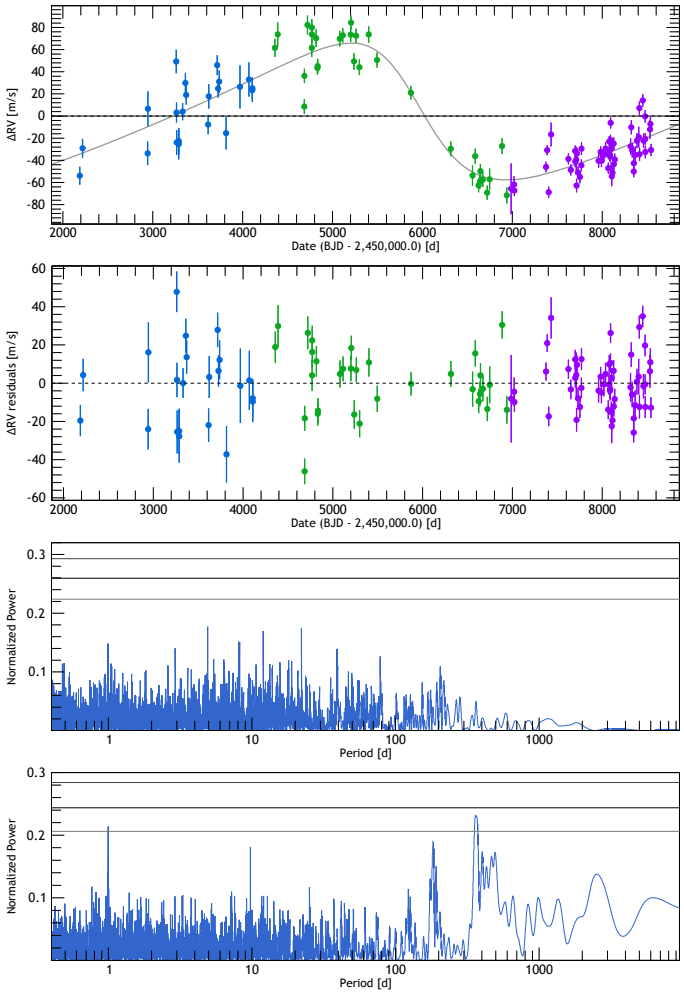


Fig. 3. *Top*: HD 25015 RV measurements as a function of Julian Date obtained with CORALIE-98 (blue), CORALIE-07 (green) and CORALIE-14 (purple). The fitted single-planet Keplerian model is represented as a black curve. *Second figure*: RV residuals of HD 25015. *Third figure*: periodogram of the residuals for HD 25015 after the signal has been removed showing no significant signals. The three black lines represent the 10, 1 and 0.1% FAPs in ascending order. *Bottom*: periodogram of H_α before detrending. The three black lines represent the 10, 1 and 0.1% FAPs in ascending order, showing a significant peak above the 10% FAP at 370.26 days.

before detrending. The results from the fully probed parameter space from the MCMC are shown in the appendix.

3.4. HD 13724 (HIP 10278)

HD 13724 has been observed with CORALIE at La Silla Observatory since August 1999. It is a relatively young star at 0.76 ± 0.71 Gyr old.

During the past 19.3 yr, 167 Doppler measurements were taken on this target with 70 RV measurements taken with CORALIE-98, 19 with CORALIE-07, 48 with CORALIE-14 and 30 with HARPS. HD 13724b is a brown dwarf companion with a minimum mass of 26.77 $M_{\rm Jup}$ and a semi-major axis of 12.4 AU, making it a promising candidate for direct imaging.

The orbital solutions for HD 13724 are summarised in Table 3. Figure 4 shows the CORALIE RVs and the corresponding best-fit Keplerian model along with the RV residuals and a periodogram of the residuals. The results from the fully probed parameter space from the MCMC are shown in the appendix.

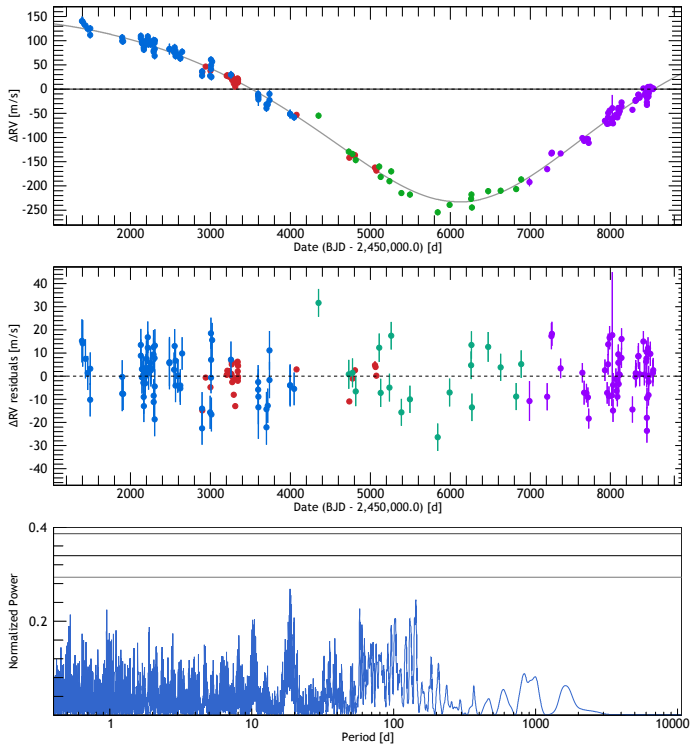


Fig. 4. *Top*: HD 13724 RV measurements as a function of Julian Date obtained with CORALIE-98 (blue), CORALIE-07 (green), CORALIE-14 (purple) and HARPS (red). The best single-planet Keplerian model is represented as a black curve. *Middle*: RV residuals of HD 13724. *Bottom*: periodogram of the residuals for HD 13724 after the signal has been removed showing no significant signals. The three black lines represent the 10, 1 and 0.1% FAPs in ascending order.

4. Updated parameters for known exoplanets

We present updated orbital parameters for a known exoplanet around HD 98649 (Marmier et al. 2013). We also report updated orbital parameters for HD 92788b (Fischer et al. 2001) and confirm the detection of HD 92788c (Wittenmyer et al. 2019). Moreover, we report the discovery of a new planet around HD 50499 and report updated orbital parameters for HD 50499b (Vogt et al. 2005).

The RV data is fitted in the same way as described in Sect. 3. The stellar parameters for these systems are summarised in Table 1. For HD 50499 we also report the discovery of a new exoplanet.

The orbital parameters for HD 98649, HD 50499, and HD 92788 are summarised in Table 4. The probed physical parameters using the MCMC for each target are shown in the appendix.

4.1. A companion of 7 $M_{\rm Jup}$ on an eccentric orbit of 15 yr around HD 98649 (LTT 4199, HIP 55409)

We report updated parameters for a known exoplanet detected by Marmier et al. (2013). The star HD 98649 is of G3/G5V type at 42.19 ± 0.09 pc from the Sun. The star properties are summarised in Table 4.

HD 98649 has been observed with CORALIE at La Silla Observatory since February 2003. Fourteen measurements were taken with CORALIE-98, 42 additional RV measurements were obtained with CORALIE-07, followed by 12 additional RV measurements obtained with CORALIE-14.

Table 4. Best-fitted solution for the substellar companions orbiting HD 50499, HD 92788, and HD 98649.

Parameters	Units	HD 50499b	HD 50499c	HD 92788b	HD 92788c	HD 98649b
P	(yr)	6.80 ± 0.05	$23.6^{+7.18}_{-1.11}$	0.892 ± 0.0001	$31.79^{+13.84}_{-2.48}$	$16.49^{+1.13}_{-0.70}$
K	(ms^{-1})	$18.94^{+0.82}_{-0.86}$	$24.23^{+3.79}_{-0.95}$	$108.24^{+0.89}_{-0.84}$	$33.29^{+2.33}_{-1.94}$	$140.1^{+33.1}_{-6.1}$
e		$0.27^{+0.04}_{-0.03}$	$0.00^{+0.14}_{-0.02}$	$0.35^{+0.004}_{-0.005}$	$0.46^{+0.12}_{-0.03}$	$0.86^{+0.04}_{-0.02}$
ω	(deg)	$259.32^{+7.89}_{-10.19}$	$[-115, +161]$	$-82.17^{+1.01}_{-1.16}$	$-25.71^{+6.63}_{-8.92}$	$252.61^{+1.97}_{-7.03}$
T_p	(JD)	$6172.9^{+50.4}_{-67.5}$	11832^{+3731}_{-2885}	$5647.14^{+0.73}_{-0.73}$	6858^{+133}_{-202}	$5121.7^{+16.8}_{-28.1}$
$M. \sin i$	(M_{Jup})	1.45 ± 0.08	$2.93^{+0.73}_{-0.18}$	$3.76^{+0.16}_{-0.15}$	$3.67^{+0.30}_{-0.25}$	$6.79^{+0.53}_{-0.31}$
a	(AU)	3.93 ± 0.07	$9.02^{+1.73}_{-0.33}$	0.97 ± 0.02	$10.50^{+2.90}_{-0.55}$	$6.57^{+0.31}_{-0.23}$
N_{RV}		214		214		68
ΔT	(yr)	19.9		18.8		15.8

Notes. For each parameter, the mode of the posterior is considered, with error bars computed from the MCMC chains with 10 000 000 iterations using a 68.27% confidence interval. ΔT is the time interval between the first and last measurements. C98 stands for CORALIE-98, C07 for CORALIE-07, and C14 for CORALIE-14. N_{RV} is the number of RV measurements. Because the ω for HD 50499c is not very well constrained, we only provide the 68.27% confidence interval here. The fully probed parameters from the MCMC can be found in the appendix. T_p is shown in BJD-2 450 000.

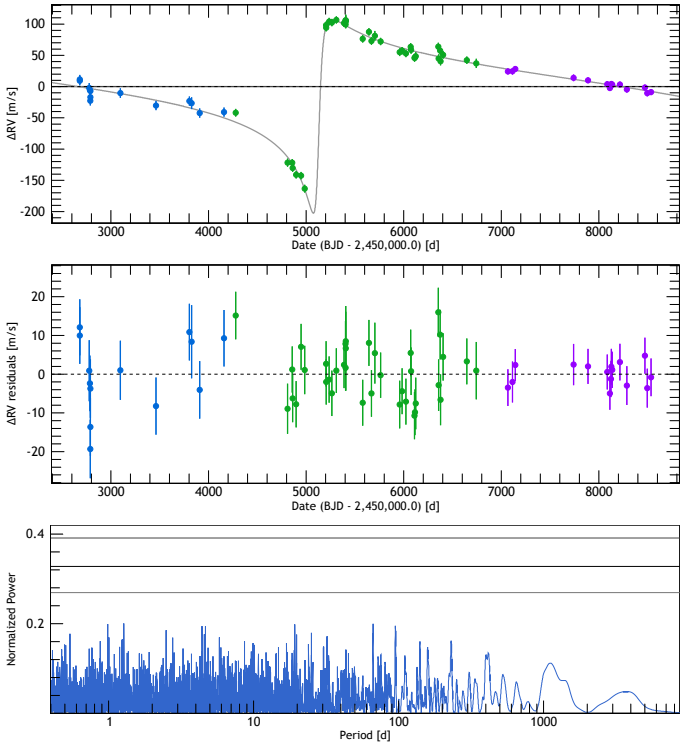


Fig. 5. *Top*: HD 98649 RV measurements as a function of Julian Date obtained with CORALIE-98 (blue), CORALIE-07 (green) and CORALIE-14 (purple). The best single-planet Keplerian model is represented as a black curve. *Middle*: RV residuals of HD 98649. *Bottom*: periodogram of the residuals for HD 98649 showing no significant signals remaining. The three black lines represent the 10, 1 and 0.1% FAP in ascending order.

HD 98649b is an extremely eccentric planet with an eccentricity of $0.86^{+0.04}_{-0.02}$. The orbital parameters agree well with Marmier et al. (2013) who reported a period of $P = 13.56^{+1.66}_{-1.27}$ yr and a mass of $M \sin i = 6.8 \pm 0.5\ M_{Jup}$.

The orbital solutions for HD 98649 are summarised in Table 4. Figure 5 shows the CORALIE RVs and the corresponding best-fit Keplerian model along with the RV residuals and a periodogram of the residuals. The results from the fully probed parameter space from the MCMC are shown in the appendix.

4.2. HD 50499 (HIP 32970)

HD 50499 is a G1V star at 46.34 ± 0.06 pc from the Sun. The star properties are summarised in Table 1.

We report updated orbital parameters for a known exoplanet around HD 50499b previously detected by Vogt et al. (2005). We also report the discovery of a new exoplanet in this system.

HD 50499 was observed with CORALIE at La Silla Observatory since January 1999. Forty-four measurements were taken with CORALIE-98, 39 additional RV measurements with CORALIE-07, followed by 40 additional RV measurements obtained with CORALIE-14. There are also 5 measurements taken with HARPS, as well as an additional 86 RV points publicly available from HIRES.

The outer signal was previously noted by Vogt et al. (2005). It was also reported by Butler et al. (2017) who noted that the outer trend is parabolic with additional data points from HIRES. In addition, Barbato et al. (2018) fits the RV data for a single Keplerian orbit plus a quadratic term obtaining a best-fit curve where lower limits for the outer companion are derived. Here we provide additional data points from CORALIE, which allows us to further constrain this outer planet.

We derive the orbital solution for HD 50499 using two Keplerians as seen in Fig. 6. The orbital solutions for HD 50499 are summarised in Table 4. Figure 6 shows the CORALIE, HARPS, and HIRES RVs and the corresponding best-fit Keplerian models along with the periodogram of the residuals. Figure 7 shows the phase-folded RV diagrams for HD 50499b and HD 50499c. The results from the fully probed parameter space from the MCMC are shown in the appendix.

These parameters agree well with Vogt et al. (2005) who reports that HD 50499b has a period of 6.80 ± 0.30 yr and a mass of $1.71 \pm 0.2\ M_{Jup}$.

Because not all of the outer planet period is covered, the uncertainties on the period of the second Keplerian remain relatively large with an unconstrained ω.

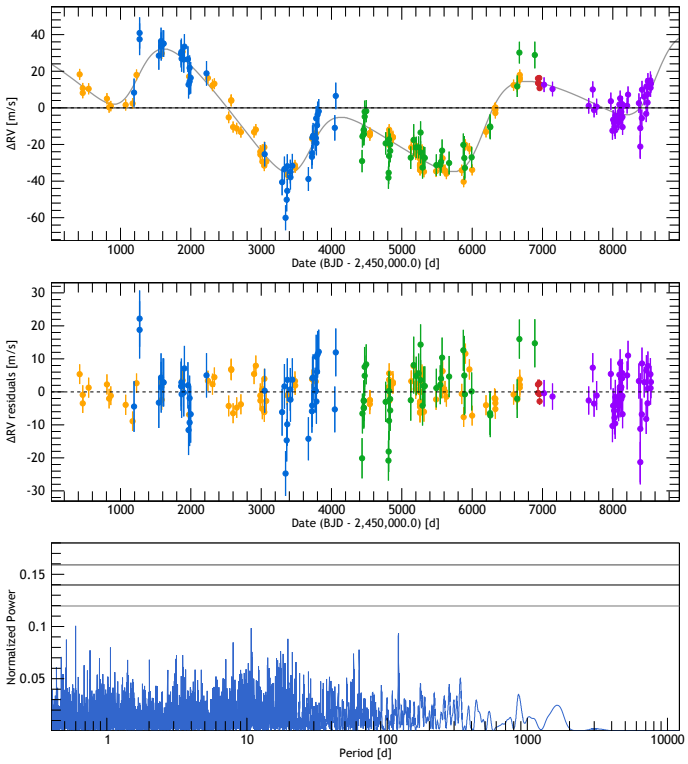


Fig. 6. *Top*: HD 50499 RV curves. Blue: CORALIE-98 data; green: CORALIE-07; purple: CORALIE-14 data; red: HARPS data; and orange: HIRES data (Butler et al. 2017). The Keplerian models are represented by black curves. *Middle*: RV residuals of HD 50499. *Bottom*: periodogram of the residuals of HD 50499 after the two planetary signals were removed, indicating that there are no more significant signals remaining in the data. The three black lines represent the 10, 1 and 0.1% FAPs in ascending order.

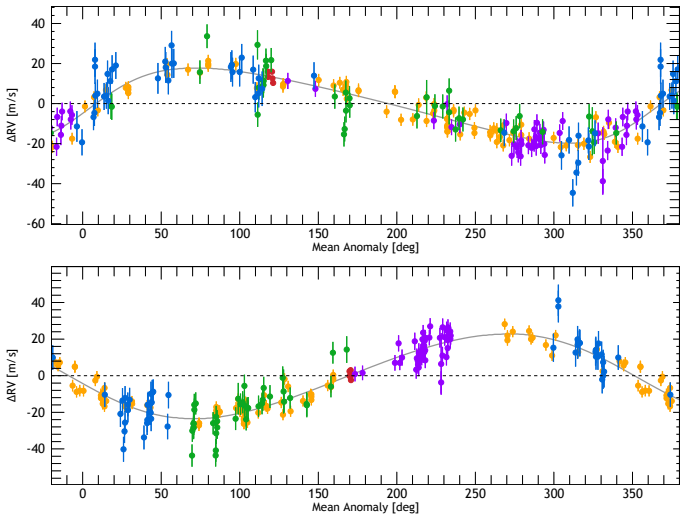


Fig. 7. Phase-folded RV curves for HD 50499. Blue: CORALIE-98 data; green: CORALIE-07; purple: CORALIE-14 data; red: HARPS data; orange: HIRES data. The Keplerian models are represented by black curves. *Top*: phase-folded curve for HD 50499b. *Bottom*: phase-folded curve for HD 50499c.

The parameters we obtain for HD 50499c agree with Barbato et al. (2018) who report that the quadratic trend corresponds to a planet with an orbital period of $P \geq 22.61$ yr and a minimum mass of $M \sin i \geq 0.942\, M_{\rm Jup}$.

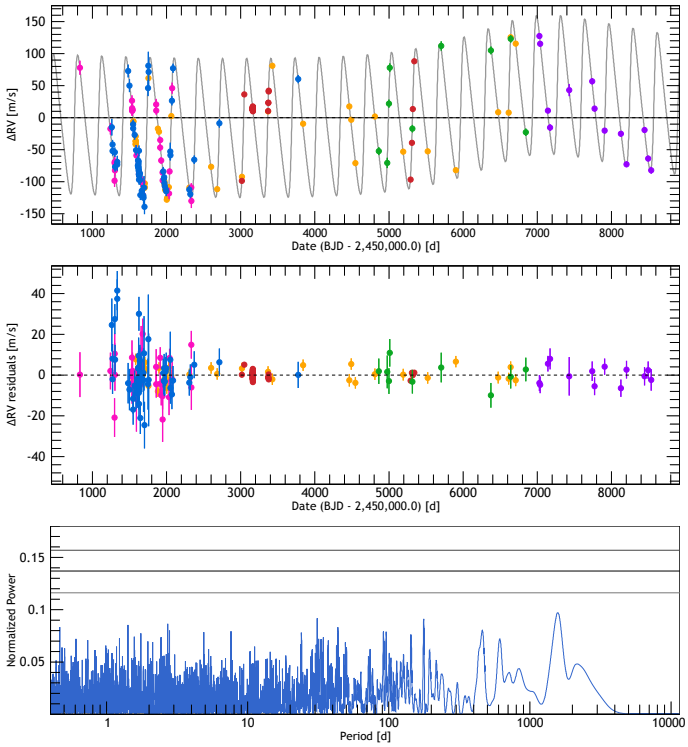


Fig. 8. *Top*: HD 92788 RV measurements as a function of Julian Date obtained with CORALIE-98 (blue), CORALIE-07 (green), CORALIE-14 (purple), HARPS (red), HIRES (orange; Butler et al. 2017) and HAMILTON (pink; Butler et al. 2006). The best single-planet Keplerian model is represented by black curve. *Middle*: RV residuals of HD 92788. *Bottom*: periodogram of the residuals for HD 92788 after the signal was removed showing no significant signals. The three black lines represent the 10, 1, and 0.1% FAPs in ascending order.

4.3. HD 92788 (HIP 52409)

We report updated orbital parameters for HD 92788b (Fischer et al. 2001) and confirm the detection of HD 92788c (Wittenmyer et al. 2019). HD 92788 is a G6V star at 28.83 ± 0.05 pc from the Sun. The star properties are summarised in Table 4.

HD 92788 was observed with CORALIE at La Silla Observatory since March 1999, 59 RV measurements were obtained with CORALIE-98, an additional 10 RV measurements were obtained with CORALIE-07, and an additional 11 RV measurements were obtained with CORALIE-14. There are also 61 measurements taken with HARPS, 42 RV points publicly available from HIRE, and an additional 31 RV points from HAMILTON.

The orbital solutions for HD 92788 are summarised in Table 4. Figure 8 shows the CORALIE, HARPS, HIRES, and HAMILTON RVs and the corresponding best-fit Keplerian models along with a time series of the residuals and a periodogram of the residuals. Figure 9 shows the phase-folded RV diagram for HD 92788b and the time series for HD 92788c. The results from the fully probed parameter space from the MCMC are shown in the appendix.

The orbital parameters for HD 92788b agree well with Fischer et al. (2001) who reported a period of $P = 0.894 \pm 0.009$ yr and a minimum mass of $M \sin i = 3.34\, M_{\rm Jup}$ and also agree well with the recently reported parameters by Wittenmyer et al. (2019) who report HD 92788b to have an orbital period of 0.892 ± 0.00008 yr and a minimum mass of $M \sin i = 3.78 \pm 0.18 M_{\rm Jup}$.

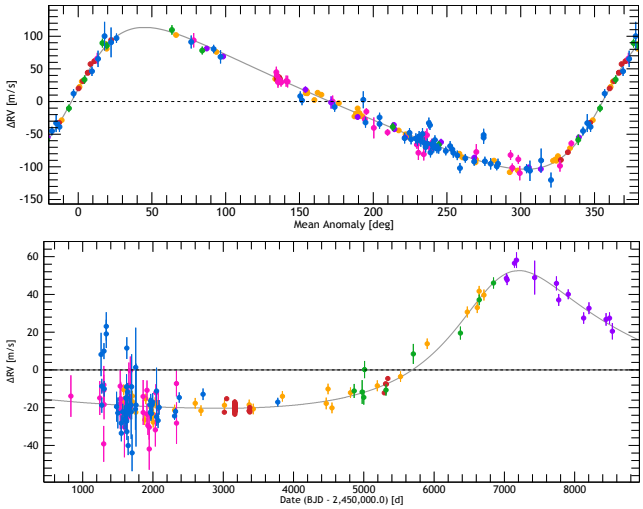


Fig. 9. Blue: CORALIE-98 data; green: CORALIE-07 data; purple: CORALIE-14 data; red: HARPS data; orange: HIRES data; pink: HAMILTON data. The Keplerian models are represented by black curves. *Top*: phase-folded curve for HD 92788b. *Bottom*: time series for HD 92788c.

Wittenmyer et al. (2013) tested the system for a potential additional planet with a period of 162 days which they found by limiting the eccentricity of the Keplerian model of HD 92788b. This is because fitting Keplerians can be biased towards fitting an increased eccentricity, especially when the semi-amplitude is small or the system has not been sampled well (Shen & Turner 2008). Although Wittenmyer et al. (2013) suggested that there is a possible additional planet in the system, when we fitted the Keplerian the signal was not significant above the noise (lower than a 10% FAP) to claim an additional planet at this period, as seen in Fig. 8 and therefore we do not detect this signal.

We do however detect the signal of another planet in the system, HD 92788c, as was recently discovered by Wittenmyer et al. (2019). We confirm this planet with orbital parameters that agree with Wittenmyer et al. (2019), who report a period of 26.99 ± 2.54 yr and a minimum mass of $M \sin i$ of 3.64 ± 0.69 $M_{\rm Jup}$.

5. Discussion and conclusion

Here we report the discovery of five new giant planets and brown dwarf candidates discovered with the CORALIE spectrograph mounted on 1.2 m Euler Swiss telescope at La Silla Observatory as well as updated orbital parameters for four previously detected planets. CORALIE time series combined with the published data sets independently confirms the existence of these four already published companions. In addition, we do not find any significant evidence for the exoplanet HD 92788c suggested by Wittenmyer et al. (2013). The newly reported companions span a period range of 15.6–40.4 yr and a mass domain of 2.93–26.77 $M_{\rm Jup}$.

Most of the parent stars in this paper have a metallicity excess, as seen in Fig. 10. Despite the small size of our sample, our results seem to agree with previous observations that giant planets appear to occur significantly around stars that are more metal-rich, which has been noted before by Santos et al. (2004), Fischer & Valenti (2005), Mayor et al. (2011) and Boisse et al. (2012).

The focus of this paper is on long-period exoplanets, where all of the newly reported planets have periods over 15 yr. This contributes to the relatively small number of previously known planets with periods in this range, where according to the NASA

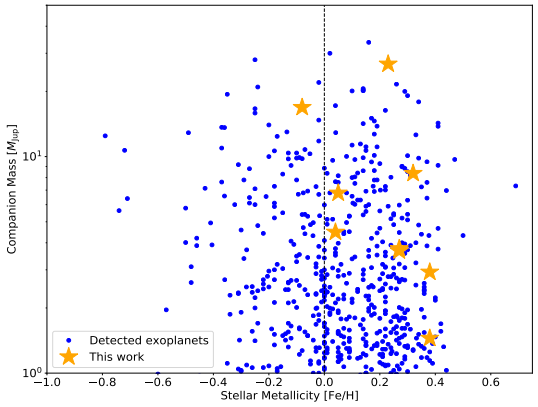


Fig. 10. Companion mass in the limits 1–50 $M_{\rm Jup}$ as a function of the host star metallicity. The new companions presented in this paper are shown by the orange stars. Previously detected planets and brown dwarfs are shown in blue[2]. The black dashed line shows the metallicity of the Sun. Most of the stars with detected companions in this paper have a significant metallicity excess.

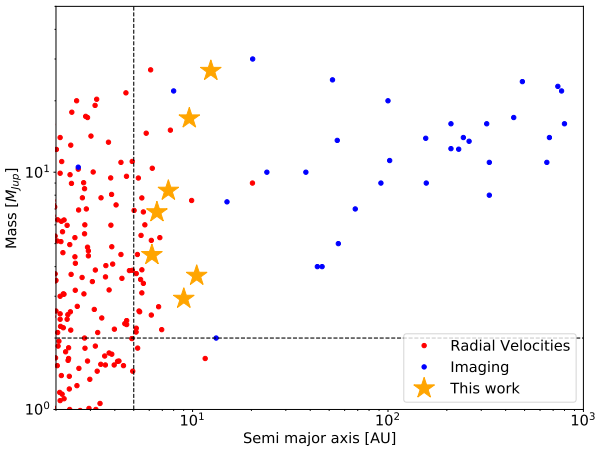


Fig. 11. Mass of detected exoplanets and brown dwarfs as a function of separation. The new companions presented in this paper are shown by the orange stars. Previously detected imaged planets and brown dwarfs are shown in blue and the RV-detected planets are shown in red[2]. The black dashed lines show the limits for companions that are in a potential detectable parameter space with imaging, i.e., giant planets more massive than 2 $M_{\rm Jup}$ and planets at a separation larger than 5 AU.

Exoplanet Archive[3] there are only 26 known exoplanets with a period greater than 15 yr.

As seen in Fig. 11, the planets and brown dwarfs presented in this paper are bridging the gap between the RV detected exoplanets and the directly imaged exoplanets. As we achieve deeper detection limits and smaller inner working angles in imaging with new instrumentation and telescopes, and span longer base lines with RV techniques, this gap in separation will decrease.

Combining RV and direct imaging data has previously been done, for example by Kane et al. (2014), Rodigas et al. (2016a,b) and Crepp et al. (2012). More recently, these two techniques have been combined for two candidates from the CORALIE RV survey with the detection of HD 4747 B by Peretti et al. (2019) and with the discovery of an ultra-cool brown dwarf companion to HD 4113 A by Cheetham et al. (2018).

[2] Companions taken from the NASA Exoplanet Archive.
[3] The NASA Exoplanet Archive can be accessed at https://exoplanetarchive.ipac.caltech.edu/index.html

With future direct imaging detections of these candidates presented here, we aim to follow the same method as Cheetham et al. (2018) and Peretti et al. (2019), and perform an atmospheric retrieval analysis of carbon and oxygen abundances, as demonstrated by Lavie et al. (2017). The CORALIE survey plays an important step in identifying promising targets for such observations, making CORALIE a unique instrument in being able to carry out such a long continuous survey at high precision. Furthermore, the stars in the CORALIE sample are older than the commonly and directly imaged targets, and so the substellar companions probed in this paper represent a new and complementary parameter space.

A great many attempts have been made to detect these long-period companions through imaging as part of a 15-yr effort using VLT/NACO with little success. Now with the capabilities of VLT/SPHERE with a contrast limit of $\sim 10^{-3}$–10^{-4} at a separation of 0.1 arcsec (Beuzit et al. 2019) we are able to start detecting these massive planets and brown dwarfs.

Some of these targets may be challenging for SPHERE, but where this is the case, they should be within the capabilities of ELT/METIS, where METIS should achieve a 10^{-5} contrast at 0.1 arcseconds (Carlomagno et al. 2016). In addition, combining astrometry that will be available from *Gaia* with RV data will allow us to further constrain the range of possible masses of these massive companions.

Acknowledgements. This work has been carried out within the framework of the National Centre for Competence in Research PlanetS supported by the Swiss National Science Foundation. The authors acknowledge the financial support of the SNSF. This publication makes use of the Data & Analysis Center for Exoplanets (DACE), which is a facility based at the University of Geneva (CH) dedicated to extrasolar planets data visualisation, exchange and analysis. DACE is a platform of the Swiss National Centre of Competence in Research (NCCR) PlanetS, federating the Swiss expertise in Exoplanet research. The DACE platform is available at https://dace.unige.ch. L.A.dS. and J.V.S. acknowledge the support from the European Research Council (ERC) under the European Union's Horizon 2020 research and innovation programme (project FOUR ACES, grant agreement No 724427). N.C.S. was supported by FCT – Fundação para a Ciência e a Tecnologia – through national funds and by FEDER through COMPETE2020 – Programa Operacional Competitividade e Internacionalização by these grants: UID/FIS/04434/2013 & POCI-01-0145-FEDER-007672; PTDC/FIS-AST/28953/2017 & POCI-01-0145-FEDER-028953 and PTDC/FIS-AST/32113/2017 & POCI-01-0145-FEDER-032113. This work has made use of data from the European Space Agency (ESA) mission *Gaia* (http://www.cosmos.esa.int/gaia), processed by the *Gaia* Data Processing and Analysis Consortium (DPAC, http://www.cosmos.esa.int/web/gaia/dpac/consortium). Funding for the DPAC has been provided by national institutions, in particular the institutions participating in the *Gaia* Multilateral Agreement.

References

Baluev, R. V. 2008, MNRAS, 385, 1279
Barbato, D., Sozzetti, A., Desidera, S., et al. 2018, A&A, 615, A175
Beuzit, J.-L., Vigan, A., Mouillet, D., et al. 2019, A&A, submitted, [arXiv:1902.04080]
Boisse, I., Pepe, F., Perrier, C., et al. 2012, A&A, 545, A55
Bond, J. C., Tinney, C. G., Butler, R. P., et al. 2006, MNRAS, 370, 163
Bowler, B. P. 2016, PASP, 128, 102001
Butler, R. P., Wright, J. T., Marcy, G. W., et al. 2006, ApJ, 646, 505
Butler, R. P., Vogt, S. S., Laughlin, G., et al. 2017, AJ, 153, 208
Carlomagno, B., Absil, O., Kenworthy, M., et al. 2016, in Adaptive Optics Systems V, Proc. SPIE, 9909, 990973
Cheetham, A., Ségransan, D., Peretti, S., et al. 2018, A&A, 614, A16
Crepp, J. R., Johnson, J. A., Howard, A. W., et al. 2012, ApJ, 761, 39
Crepp, J. R., Principe, D. A., Wolff, S., et al. 2018, ApJ, 853, 192
Delisle, J. B., Ségransan, D., Buchschacher, N., & Alesina, F. 2016, A&A, 590, A134
Delisle, J.-B., Ségransan, D., Dumusque, X., et al. 2018, A&A, 614, A133
Díaz, R. F., Almenara, J. M., Santerne, A., et al. 2014, MNRAS, 441, 983
Díaz, R. F., Ségransan, D., Udry, S., et al. 2016, A&A, 585, A134
Ekström, S., Georgy, C., Eggenberger, P., et al. 2012, A&A, 537, A146
Feigelson, E. D., Lawson, W. A., Stark, M., Townsley, L., & Garmire, G. P. 2006, AJ, 131, 1730
Fischer, D. A., & Valenti, J. 2005, ApJ, 622, 1102
Fischer, D. A., Marcy, G. W., Butler, R. P., et al. 2001, ApJ, 551, 1107
Fischer, D. A., Howard, A. W., Laughlin, G. P., et al. 2014, Protostars and Planets VI (Tucson: University of Arizona Press), 715
Gaia Collaboration (Brown, A. G. A., et al.) 2018, A&A, 616, A1
Georgy, C., Ekström, S., Eggenberger, P., et al. 2013, A&A, 558, A103
Gomes da Silva, J., Santos, N. C., Boisse, I., Dumusque, X., & Lovis, C. 2014, A&A, 566, A66
Kane, S. R., Howell, S. B., Horch, E. P., et al. 2014, ApJ, 785, 93
Lavie, B., Mendonça, J. M., Mordasini, C., et al. 2017, AJ, 154, 91
Mamajek, E. E., & Hillenbrand, L. A. 2008, ApJ, 687, 1264
Marmier, M. 2014, Ph.D. Thesis, Geneva Observatory, University of Geneva, Switzerland
Marmier, M., Ségransan, D., Udry, S., et al. 2013, A&A, 551, A90
Mayor, M., Pepe, F., Queloz, D., et al. 2003, The Messenger, 114, 20
Mayor, M., Marmier, M., Lovis, C., et al. 2011, ArXiv e-prints [arXiv:1109.2497]
Pepe, F., Mayor, M., Galland, F., et al. 2002, A&A, 388, 632
Peretti, S., Ségransan, D., Lavie, B., et al. 2019, A&A, accepted [arXiv:1805.05645]
Perryman, M. A. C., Lindegren, L., Kovalevsky, J., et al. 1997, A&A, 323, L49
Porto de Mello, G. F., da Silva, R., da Silva, L., & de Nader, R. V. 2014, A&A, 563, A52
Rodigas, T. J., Bergeron, P., Simon, A., et al. 2016a, ApJ, 831, 177
Rodigas, T. J., Arriagada, P., Faherty, J., et al. 2016b, ApJ, 818, 106
Santos, N. C., Israelian, G., & Mayor, M. 2001, A&A, 373, 1019
Santos, N. C., Israelian, G., & Mayor, M. 2004, A&A, 415, 1153
Santos, N. C., Sousa, S. G., Mortier, A., et al. 2013, A&A, 556, A150
Ségransan, D., Udry, S., Mayor, M., et al. 2010, A&A, 511, A45
Shen, Y., & Turner, E. L. 2008, ApJ, 685, 553
Sousa, S. G., Santos, N. C., Mayor, M., et al. 2008, A&A, 487, 373
Tamuz, O., Ségransan, D., Udry, S., et al. 2008, A&A, 480, L33
Udry, S., Mayor, M., Naef, D., et al. 2000, A&A, 356, 590
Udry, S., Mayor, M., Naef, D., et al. 2002, A&A, 390, 267
Vogt, S. S. 1987, PASP, 99, 1214
Vogt, S. S., Allen, S. L., Bigelow, B. C., et al. 1994, in Instrumentation in Astronomy VIII, eds. D. L. Crawford, & E. R. Craine, Proc. SPIE, 2198, 362
Vogt, S. S., Butler, R. P., Marcy, G. W., et al. 2005, ApJ, 632, 638
Wittenmyer, R. A., Wang, S., Horner, J., et al. 2013, ApJS, 208, 2
Wittenmyer, R. A., Clark, J. T., Zhao, J., et al. 2019, MNRAS, 484, 5859
Zuckerman, B., Song, I., Bessell, M. S., & Webb, R. A. 2001, ApJ, 562, L87
Zuckerman, B., Rhee, J. H., Song, I., & Bessell, M. S. 2011, ApJ, 732, 61

[1] Département d'astronomie, Université de Genève, 51 ch. des Maillettes, 1290 Versoix, Switzerland
e-mail: emily.rickman@unige.ch
[2] Instituto de Astrofísica e Ciências do Espaço, Universidade do Porto, CAUP, Rua das Estrelas, 4150-762 Porto, Portugal
[3] Departamento de Física e Astronomia, Faculdade de Ciências, Universidade do Porto, Rua do Campo Alegre, 4169-007 Porto, Portugal
[4] Institute of Physics, Laboratory of Astrophysics, École Polytechnique Fédérale de Lausanne (EPFL), Observatoire de Sauverny, 1290, Versoix, Switzerland
[5] European Southern Observatory, Alonso de Córdova 3107, Vitacura, Santiago, Chile
[6] Department of Astronomy and Astrophysics, University of Chicago, 5640 South Ellis Avenue, Chicago, IL 60637, USA
[7] Department of Physics, University of Warwick, Coventry CV4 7AL, UK
[8] Aix Marseille Université, CNRS, LAM (Laboratoire d'Astrophysique de Marseille) UMR 7326, 13388 Marseille, France
[9] Carnegie Institution for Science, Las Campanas Observatory, Casilla 601, Colina El Pino s/n, La Serena, Chile
[10] Physikalisches Institut, Universität Bern, Gesellschaftsstr. 6, 3012 Bern, Switzerland
[11] Instituto de Astrofísica de Canarias, 38205 La Laguna, Tenerife, Spain
[12] School of Physics & Astronomy, University of Birmingham, Edgbaston, Birmingham, B15 2TT, UK
[13] Leiden Observatory, Leiden University, Postbus 9513, 2300 RA Leiden, Netherlands

Appendix A: Direct access to the RVs and other data products

The RV measurements and additional data products discussed in this paper are available in electronic form on the DACE web platform for each individual target with each link. A copy of the data is also available at the CDS.

HD 13724: https://dace.unige.ch/radialVelocities/?pattern=HD13724
HD 181234: https://dace.unige.ch/radialVelocities/?pattern=HD181234
HD 25015: https://dace.unige.ch/radialVelocities/?pattern=HD25015
HD 50499: https://dace.unige.ch/radialVelocities/?pattern=HD50499
HD 92788: https://dace.unige.ch/radialVelocities/?pattern=HD92788
HD 92987: https://dace.unige.ch/radialVelocities/?pattern=HD92987
HD 98649: https://dace.unige.ch/radialVelocities/?pattern=HD98649

Appendix B: MCMC tables

We probed the model parameter space with the MCMC sampler described in (Díaz et al. 2014, 2016). For each MCMC simulation, we performed 10 000 000 iterations with initial conditions drawn from the solution obtained using DACE. The corresponding parameters and confidence intervals for each star are listed in Tables B.1–B.7 for HD 181234, HD 92987, HD 13724, HD 25015, HD 98649, HD 50499 and HD 92788 respectively.

Table B.1. Parameters probed by the MCMC used to fit the RV measurements of HD 181234.

Parameter	Units	Max(likelihood)	Mode	Mean	Std	Median	68.27%	95.45%	99.73%	Prior
log(likelihood)		−359.29	−365.26	−366.31	2.83	−365.95	[−369.09–363.55]	[−372.93–361.77]	[−377.96–360.46]	–
Star										
M_S	($M_\odot$)	1.0495	1.0117	1.0101	0.0601	1.0105	[0.9501–1.0704]	[0.8899–1.1296]	[0.8287–1.1895]	$\mathcal{U}$
Π_S	(mas)	21.093	20.916	20.915	0.209	20.915	[20.708–21.123]	[20.498–21.336]	[20.280–21.538]	$\mathcal{U}$
Offset										
$\gamma_{\mathrm{COR98(DRS-3.3)}}$	(m s^{-1})	−8.36	−5.47	−5.41	2.74	−5.44	[−8.14–2.69]	[−10.79–0.22]	[−13.61–3.38]	$\mathcal{N}(0,4)$
$\gamma_{\mathrm{HIRES(Pub-2017)}}$	(m s^{-1})	46701.91	46703.49	46703.39	2.42	46703.40	[46701.00–46705.79]	[46698.55–46708.24]	[46695.72–46711.05]	$\mathcal{U}$
$\gamma_{\mathrm{COR07(DRS-3.4)}}$	(m s^{-1})	−46664.21	−46664.26	−46664.23	1.99	−46664.23	[−46666.21–46662.23]	[−46668.23–46660.32]	[−46670.43–46658.23]	$\mathcal{U}$
$\gamma_{\mathrm{COR14(DRS-3.8)}}$	(m s^{-1})	15.82	14.32	14.40	3.31	14.38	[11.08–17.72]	[7.84–21.08]	[4.93–24.60]	$\mathcal{N}(12,4)$
Noise										
$\sigma_{\mathrm{COR98(DRS-3.3)}}$	(m s^{-1})	5.52	7.12	8.04	2.82	7.70	[5.40–10.67]	[3.39–14.71]	[1.18–20.48]	$\mathcal{U}$
$\sigma_{\mathrm{COR07(DRS-3.4)}}$	(m s^{-1})	8.13	8.15	8.82	2.14	8.57	[6.77–10.84]	[5.34–13.84]	[4.10–17.95]	$\mathcal{U}$
$\sigma_{\mathrm{HIRES(Pub-2017)}}$	(m s^{-1})	2.966	3.265	3.555	0.790	3.453	[2.803–4.300]	[2.287–5.447]	[1.845–6.988]	$\mathcal{U}$
$\sigma_{\mathrm{COR14(DRS-3.8)}}$	(m s^{-1})	2.846	3.378	3.413	0.815	3.394	[2.631–4.205]	[1.810–5.122]	[0.703–6.113]	$\mathcal{U}$
HD 181234b										
P	(d)	7515.1	7463.4	7465.4	80.7	7464.3	[7385.6–7545.4]	[7307.0–7632.1]	[7221.7–7718.5]	$\mathcal{U}$
K	(m s^{-1})	126.31	126.75	126.81	1.71	126.77	[125.11–128.52]	[123.49–130.32]	[122.00–132.26]	$\mathcal{U}$
e		0.72845	0.73177	0.73216	0.00710	0.73211	[0.72512–0.73925]	[0.71793–0.74649]	[0.71028–0.75311]	$\mathcal{U}$
ω	(°)	94.75	93.27	93.23	1.78	93.24	[91.46–95.01]	[89.62–96.75]	[87.88–98.58]	$\mathcal{U}$
T_{Vmin}	(BJD)	2460630.87	2457946.63	2457946.37	8.55	2457946.40	[2457937.94–2457954.82]	[2457928.94–2457963.58]	[2457919.90–2457972.50]	$\mathcal{U}$
a_S	(AU)	0.05978	0.05922	0.05926	0.00110	0.05925	[0.05816–0.06036]	[0.05711–0.06153]	[0.05605–0.06275]	–
a	(AU)	7.650	7.517	7.517	0.159	7.519	[7.359–7.676]	[7.192–7.828]	[7.019–7.976]	–
m	($M_\oplus$)	2737	2659	2656	111	2657	[2544–2767]	[2430–2877]	[2318–2986]	–
m	(M_J)	8.613	8.366	8.358	0.351	8.361	[8.006–8.707]	[7.648–9.053]	[7.294–9.395]	–
m	($M_\odot$)	0.008222	0.007986	0.007978	0.000335	0.007980	[0.007641–0.008311]	[0.007300–0.008641]	[0.006962–0.008968]	–
T_C	(BJD)	2460344.43	2457661.70	2457661.72	2.36	2457661.72	[2457659.38–2457664.06]	[2457656.97–2457666.45]	[2457654.32–2457669.15]	–
T_P	(BJD)	2460355.10	2457668.66	2457668.91	5.26	2457668.85	[2457663.69–2457674.13]	[2457658.52–2457679.58]	[2457653.25–2457685.35]	–

Notes. The maximum likelihood solution, median, mode, and standard-deviation of the posterior distribution for each parameter are shown, as well as the 68.27, 95.45, and 99.73% confidence intervals. The prior for each parameter can be of type: $\mathcal{U}$: uniform, $\mathcal{N}$: normal, or $\mathcal{TN}$: truncated normal. Reference epoch: 2455500.0 BJD.

Table B.2. Parameters probed by the MCMC used to fit the RV measurements of HD 92987.

Parameter	Units	Max(likelihood)	Mode	Mean	Std	Median	68.27%	95.45%	99.73%	Prior
log(likelihood)		−287.21	−292.23	−293.24	2.60	−292.89	[−295.76–290.72]	[−299.43–289.15]	[−303.96–288.07]	–
Star										
M_S	($M_\odot$)	1.0877	1.0795	1.0807	0.0601	1.0805	[1.0207–1.1409]	[0.9602–1.2010]	[0.9018–1.2590]	$\mathcal{U}$
Π_S	(mas)	22.860	22.943	22.943	0.228	22.944	[22.715–23.170]	[22.487–23.399]	[22.279–23.626]	$\mathcal{U}$
Offset										
$\gamma_{\mathrm{COR14(DRS-3.8)}}$	($\mathrm{m\,s^{-1}}$)	11.89	11.28	11.21	3.40	11.21	[7.80–14.61]	[4.35–18.01]	[0.77–21.33]	$\mathcal{N}(12,4)$
$\gamma_{\mathrm{COR98(DRS-3.3)}}$	($\mathrm{m\,s^{-1}}$)	10.38	5.65	5.73	2.82	5.73	[2.94–8.52]	[0.06–11.39]	[−2.92–14.40]	$\mathcal{N}(0,4)$
$\gamma_{\mathrm{COR07(DRS-3.4)}}$	($\mathrm{m\,s^{-1}}$)	4757.07	4759.04	4759.37	2.21	4759.25	[4757.21–4761.52]	[4755.31–4764.14]	[4753.41–4767.46]	$\mathcal{U}$
Noise										
$\sigma_{\mathrm{COR07(DRS-3.4)}}$	($\mathrm{m\,s^{-1}}$)	2.88	3.55	3.76	1.60	3.66	[2.25–5.26]	[0.71–7.32]	[0.03–10.30]	$\mathcal{U}$
$\sigma_{\mathrm{COR98(DRS-3.3)}}$	($\mathrm{m\,s^{-1}}$)	5.408	5.746	5.968	0.925	5.899	[5.065–6.876]	[4.315–8.029]	[3.656–9.431]	$\mathcal{U}$
$\sigma_{\mathrm{COR14(DRS-3.8)}}$	($\mathrm{m\,s^{-1}}$)	2.22	2.68	2.79	1.40	2.73	[1.38–4.13]	[0.26–5.85]	[0.02–8.18]	$\mathcal{U}$
HD 92987b										
$\log P$	(d)	4.0204	4.0150	4.0208	0.0175	4.0191	[4.0038–4.0376]	[3.9909–4.0607]	[3.9805–4.0921]	$\mathcal{U}$
$\log K$	($\mathrm{m\,s^{-1}}$)	2.17745	2.18372	2.18316	0.00709	2.18324	[2.17601–2.19025]	[2.16885–2.19710]	[2.16133–2.20394]	$\mathcal{U}$
$\sqrt{e}\cos\omega$		−0.4573	−0.4435	−0.4426	0.0260	−0.4428	[−0.4682–0.4169]	[−0.4939–0.3898]	[−0.5227–0.3615]	$\mathcal{U}$
$\sqrt{e}\sin\omega$		−0.1091	−0.1232	−0.1119	0.0580	−0.1154	[−0.1694–0.0541]	[−0.2173–0.0143]	[−0.2573-0.0857]	$\mathcal{U}$
T_{Vmin}	(BJD)	2457596.8	2457600.4	2457599.0	26.3	2457599.7	[2457573.1–2457625.1]	[2457543.7–2457649.7]	[2457513.1–2457674.0]	$\mathcal{U}$
a_S	(AU)	0.14139	0.14234	0.14371	0.00487	0.14321	[0.13900–0.14843]	[0.13550–0.15492]	[0.13232–0.16417]	–
a	(AU)	9.687	9.621	9.672	0.318	9.653	[9.362–9.981]	[9.093–10.365]	[8.849–10.841]	–
e		0.2210	0.2109	0.2125	0.0164	0.2118	[0.1966–0.2280]	[0.1817–0.2482]	[0.1657–0.2764]	–
K	($\mathrm{m\,s^{-1}}$)	150.47	152.67	152.48	2.49	152.49	[149.97–154.97]	[147.52–157.43]	[144.99–159.93]	–
ω	(°)	193.42	195.10	194.29	7.60	194.55	[186.68–201.84]	[178.30–208.69]	[169.69–214.64]	–
m	($M_\oplus$)	5312	5363	5369	214	5368	[5155–5583]	[4939–5796]	[4727–6002]	–
m	(M_J)	16.714	16.876	16.893	0.673	16.891	[16.222–17.566]	[15.541–18.238]	[14.874–18.887]	–
m	($M_\odot$)	0.015954	0.016108	0.016124	0.000643	0.016123	[0.015484–0.016767]	[0.014834–0.017409]	[0.014197–0.018028]	–
P	(d)	10482	10355	10499	428	10450	[10089–10904]	[9794–11501]	[9560–12362]	–
T_C	(BJD)	2455569.4	2455533.3	2455534.2	40.4	2455533.6	[2455493.9–2455574.5]	[2455455.4–2455617.2]	[2455416.6–2455662.2]	–
T_P	(BJD)	2457841	2457889	2457861	155	2457870	[2457708–2458015]	[2457530–2458147]	[2457331–2458264]	–

Notes. The maximum likelihood solution, median, mode, and standard-deviation of the posterior distribution for each parameter are shown, as well as the 68.27, 95.45, and 99.73% confidence intervals. The prior for each parameter can be of type: $\mathcal{U}$: uniform, $\mathcal{N}$: normal, or $\mathcal{TN}$: truncated normal. Reference epoch: 2455500.0 BJD.

Table B.3. Parameters probed by the MCMC used to fit the RV measurements of HD 13724.

Parameter	Units	Max(likelihood)	Mode	Mean	Std	Median	68.27%	95.45%	99.73%	Prior
log(likelihood)		−592.80	−599.41	−600.20	2.60	−599.89	[−602.74–597.67]	[−606.25–595.94]	[−610.74–594.59]	–
					Star					
M_S	($M_\odot$)	1.1744	1.1406	1.1397	0.0599	1.1396	[1.0798–1.1994]	[1.0202–1.2596]	[0.9580–1.3200]	$\mathcal{U}$
Π_S	(mas)	23.306	22.978	22.979	0.230	22.979	[22.749–23.208]	[22.520–23.441]	[22.302–23.663]	$\mathcal{U}$
					Offset					
$\gamma_{\mathrm{HARPS03(DRS-3.5)}}$	($\mathrm{m\,s^{-1}}$)	44.00	41.66	41.57	3.59	41.59	[37.95–45.16]	[34.40–48.71]	[30.79–52.28]	$\mathcal{U}$
$\gamma_{\mathrm{COR98(DRS-3.3)}}$	($\mathrm{m\,s^{-1}}$)	5.14	1.66	1.70	3.30	1.71	[−1.58–4.99]	[−4.97–8.25]	[−8.27–11.42]	$\mathcal{N}(0,4)$
$\gamma_{\mathrm{COR14(DRS-3.8)}}$	($\mathrm{m\,s^{-1}}$)	26.96	15.28	15.28	3.84	15.28	[11.44–19.10]	[7.57–22.90]	[3.94–26.52]	$\mathcal{N}(12,4)$
$\gamma_{\mathrm{COR07(DRS-3.4)}}$	($\mathrm{m\,s^{-1}}$)	20614.5	20597.2	20613.7	37.9	20608.9	[20578.6–20647.3]	[20549.7–20716.3]	[20535.6–20735.2]	$\mathcal{U}$
					Noise					
$\sigma_{\mathrm{COR07(DRS-3.4)}}$	($\mathrm{m\,s^{-1}}$)	12.93	13.98	15.25	3.34	14.76	[12.11–18.37]	[10.08–23.44]	[8.60–30.19]	$\mathcal{U}$
$\sigma_{\mathrm{HARPS03(DRS-3.5)}}$	($\mathrm{m\,s^{-1}}$)	5.622	5.493	5.772	0.859	5.671	[4.942–6.605]	[4.349–7.771]	[3.857–9.337]	$\mathcal{U}$
$\sigma_{\mathrm{COR14(DRS-3.8)}}$	($\mathrm{m\,s^{-1}}$)	9.75	9.98	10.29	1.36	10.17	[8.96–11.63]	[7.92–13.38]	[7.08–15.51]	$\mathcal{U}$
$\sigma_{\mathrm{COR98(DRS-3.3)}}$	($\mathrm{m\,s^{-1}}$)	8.340	8.723	8.884	0.963	8.821	[7.932–9.835]	[7.143–10.981]	[6.491–12.353]	$\mathcal{U}$
					HD 13724b					
$\log P$	(d)	4.2315	4.1727	4.2093	0.0979	4.1952	[4.1196–4.2941]	[4.0453–4.4723]	[4.0079–4.5266]	$\mathcal{U}$
$\log K$	($\mathrm{m\,s^{-1}}$)	2.3447	2.3310	2.3414	0.0330	2.3396	[2.3098–2.3725]	[2.2780–2.4195]	[2.2580–2.4389]	$\mathcal{U}$
$\sqrt{e}\cos\omega$		−0.6095	−0.5767	−0.5881	0.0621	−0.5862	[−0.6446–0.5307]	[−0.7277–0.4578]	[−0.7525–0.4045]	$\mathcal{U}$
$\sqrt{e}\sin\omega$		−0.0557	−0.0812	−0.0824	0.0201	−0.0818	[−0.1020–0.0626]	[−0.1243–0.0439]	[−0.1538–0.0237]	$\mathcal{U}$
T_{Vmin}	(BJD)	2456047.7	2456038.8	2456038.6	28.8	2456039.2	[2456009.9–2456067.5]	[2455979.1–2456093.7]	[2455943.9–2456120.6]	$\mathcal{U}$
a_S	(AU)	0.3212	0.2703	0.3157	0.0938	0.2954	[0.2367–0.3865]	[0.1889–0.6070]	[0.1679–0.6801]	–
a	(AU)	13.78	12.40	13.34	2.18	12.90	[11.47–15.04]	[10.21–19.86]	[9.56–21.73]	–
e		0.3745	0.3365	0.3569	0.0721	0.3507	[0.2896–0.4215]	[0.2214–0.5347]	[0.1776–0.5692]	–
K	($\mathrm{m\,s^{-1}}$)	221.1	214.3	220.1	16.9	218.6	[204.1–235.8]	[189.7–262.7]	[181.1–274.7]	–
ω	(°)	185.22	187.45	188.13	2.50	187.86	[185.80–190.39]	[183.96–194.14]	[182.15–199.24]	–
m	($M_\oplus$)	9184	8507	8875	1126	8747	[7810–9899]	[6972–11785]	[6404–12781]	–
m	(M_J)	28.90	26.77	27.93	3.54	27.52	[24.58–31.15]	[21.94–37.08]	[20.15–40.22]	–
m	($M_\odot$)	0.02759	0.02555	0.02666	0.00338	0.02627	[0.02346–0.02973]	[0.02094–0.03540]	[0.01923–0.03839]	–
P	(d)	17040	14764	16637	4187	15673	[13170–19684]	[11099–29669]	[10185–33620]	–
T_C	(BJD)	2453671	2453723	2453662	174	2453686	[2453505–2453826]	[2453202–2453933]	[2452980–2454008]	–
T_P	(BJD)	2456152.0	2456189.1	2456199.0	66.5	2456195.2	[2456135.4–2456261.8]	[2456076.2–2456345.7]	[2456008.8–2456458.5]	–

Notes. The maximum likelihood solution, median, mode, and standard-deviation of the posterior distribution for each parameter are shown, as well as the 68.27, 95.45, and 99.73% confidence intervals. The prior for each parameter can be of type: $\mathcal{U}$: uniform, $\mathcal{N}$: normal, or $\mathcal{TN}$: truncated normal. Reference epoch: 2455500.0 BJD.

Table B.4. Parameters probed by the MCMC used to fit the RV measurements of HD 25015.

Parameter	Units	Max(Likelihood)	Mode	Mean	Std	Median	68.27%	95.45%	99.73%	Prior
log(Likelihood)		−430.28	−435.20	−436.10	2.51	−435.77	[−438.54–433.67]	[−442.07–432.17]	[−446.55–431.20]	–
					Star					
M_S	($M_\odot$)	0.8851	0.8598	0.8599	0.0502	0.8600	[0.8097–0.9103]	[0.7591–0.9597]	[0.7098–1.0082]	$\mathcal{U}$
Π_S	(mas)	26.651	26.695	26.685	0.266	26.684	[26.418–26.952]	[26.157–27.218]	[25.893–27.491]	$\mathcal{U}$
					Offset					
$\gamma_{\mathrm{COR07(DRS-3.4)}}$	($\mathrm{m\,s^{-1}}$)	28536.61	28537.76	28537.61	2.83	28537.63	[28534.79–28540.43]	[28531.85–28543.20]	[28528.97–28545.98]	$\mathcal{U}$
$\gamma_{\mathrm{COR14(DRS-3.8)}}$	($\mathrm{m\,s^{-1}}$)	15.62	12.81	12.77	3.80	12.76	[8.96–16.57]	[5.21–20.38]	[1.55–24.36]	$\mathcal{N}(12, 4)$
$\gamma_{\mathrm{COR98(DRS-3.3)}}$	($\mathrm{m\,s^{-1}}$)	2.76	−0.01	−0.06	3.86	−0.03	[−3.93–3.79]	[−7.81–7.67]	[−11.51–11.69]	$\mathcal{N}(0, 4)$
					Activity cycle					
$A_{H_\alpha\mathrm{,Gauss.,0.1yr,lowpass}}$	($\mathrm{m\,s^{-1}}$)	7.59	6.81	6.82	4.37	6.82	[2.49–11.15]	[−1.95–15.58]	[−6.98–20.36]	$\mathcal{U}$
					Noise					
$\sigma_{\mathrm{COR07(DRS-3.4)}}$	($\mathrm{m\,s^{-1}}$)	10.26	12.07	10.77	4.79	11.17	[5.57–15.48]	[0.95–19.66]	[0.05–24.44]	$\mathcal{U}$
Low act.	($\mathrm{m\,s^{-1}}$)	8.32	10.54	8.53	3.85	9.19	[3.96–12.36]	[0.61–14.85]	[0.04–17.16]	$\mathcal{U}$
$\sigma_{H_\alpha\mathrm{,Gauss.,0.1yr,lowpass}}$	($\mathrm{m\,s^{-1}}$)	14.60	14.31	13.98	6.73	14.01	[6.90–20.61]	[1.20–27.89]	[0.06–35.04]	$\mathcal{U}$
$\sigma_{\mathrm{COR98(DRS-3.3)}}$	($\mathrm{m\,s^{-1}}$)	16.12	16.47	16.35	5.92	16.40	[10.75–21.88]	[3.47–28.45]	[0.21–36.46]	$\mathcal{U}$
$\sigma_{\mathrm{COR14(DRS-3.8)}}$	($\mathrm{m\,s^{-1}}$)	5.53	8.28	6.48	3.87	6.41	[2.03–10.71]	[0.28–13.87]	[0.02–17.05]	$\mathcal{U}$
					HD 25015b					
$\log P$	(d)	3.7879	3.7821	3.7937	0.0353	3.7888	[3.7609–3.8259]	[3.7377–3.8807]	[3.7187–3.9585]	$\mathcal{U}$
$\log K$	($\mathrm{m\,s^{-1}}$)	1.7817	1.7796	1.7788	0.0236	1.7791	[1.7558–1.8016]	[1.7300–1.8254]	[1.7011–1.8552]	$\mathcal{U}$
$\sqrt{e}\cos\omega$		0.190	0.133	0.128	0.100	0.128	[0.027–0.228]	[−0.071–0.328]	[−0.171–0.432]	$\mathcal{U}$
$\sqrt{e}\sin\omega$		0.5950	0.6088	0.6054	0.0631	0.6070	[0.5449–0.6668]	[0.4712–0.7283]	[0.3832–0.7800]	$\mathcal{U}$
T_{Vmax}	(BJD)	2455258	2455209	2455210	122	2455209	[2455090–2455329]	[2454964–2455458]	[2454827–2455591]	$\mathcal{U}$
a_S	(AU)	0.03141	0.03112	0.03144	0.00227	0.03132	[0.02924–0.03361]	[0.02730–0.03639]	[0.02526–0.04051]	–
a	(AU)	6.309	6.193	6.311	0.373	6.260	[5.966–6.642]	[5.720–7.231]	[5.509–8.115]	–
e		0.3901	0.3883	0.3969	0.0785	0.3944	[0.3200–0.4745]	[0.2454–0.5622]	[0.1699–0.6497]	–
K	($\mathrm{m\,s^{-1}}$)	60.49	60.11	60.18	3.29	60.13	[56.99–63.33]	[53.71–66.90]	[50.25–71.65]	–
ω	(°)	72.29	77.65	78.20	9.32	78.13	[69.06–87.41]	[59.46–96.93]	[49.33–107.71]	–
m	($M_\oplus$)	1469.8	1424.3	1428.1	91.6	1427.0	[1336.7–1520.0]	[1249.5–1614.0]	[1162.7–1713.7]	–
m	(M_J)	4.625	4.482	4.494	0.288	4.490	[4.206–4.783]	[3.932–5.079]	[3.659–5.392]	–
m	($M_\odot$)	0.004415	0.004278	0.004289	0.000275	0.004286	[0.004015–0.004565]	[0.003753–0.004848]	[0.003492–0.005147]	–
P	(d)	6137	6021	6239	531	6149	[5766–6697]	[5467–7598]	[5233–9090]	–
T_C	(BJD)	2455962.9	2455936.9	2455940.6	97.7	2455939.6	[2455843.2–2456038.8]	[2455745.3–2456137.5]	[2455648.1–2456230.8]	–
T_P	(BJD)	2455840	2455852	2455861	149	2455858	[2455715–2456009]	[2455568–2456166]	[2455413–2456323]	–

Notes. The maximum likelihood solution, median, mode, and standard-deviation of the posterior distribution for each parameter are shown, as well as the 68.27, 95.45, and 99.73% confidence intervals. The prior for each parameter can be of type: $\mathcal{U}$: uniform, $\mathcal{N}$: normal, or $\mathcal{TN}$: truncated normal. Reference epoch: 2455500.0 BJD.

Table B.5. Parameters probed by the MCMC used to fit the RV measurements of HD 98649.

Parameter	Units	Max(Likelihood)	Mode	Mean	Std	Median	68.27%	95.45%	99.73%	Prior
log(Likelihood)		−201.70	−207.30	−208.21	2.60	−207.89	[−210.77–205.67]	[−214.31–204.03]	[−218.55–202.86]	–
					Star					
M_S	($M_\odot$)	0.9465	1.0296	1.0300	0.0599	1.0299	[0.9701–1.0899]	[0.9105–1.1501]	[0.8513–1.2099]	$\mathcal{U}$
Π_S	(mas)	23.995	23.688	23.684	0.236	23.684	[23.448–23.921]	[23.211–24.158]	[22.967–24.390]	$\mathcal{U}$
					Offset					
$\gamma_{COR98(DRS-3.3)}$	($m\,s^{-1}$)	−7.05	−1.94	−1.87	3.41	−1.87	[−5.29–1.52]	[−8.66–5.01]	[−11.97–8.58]	$\mathcal{N}(0, 4)$
$\gamma_{COR14(DRS-3.8)}$	($m\,s^{-1}$)	20.61	16.33	16.18	2.86	16.22	[13.33–19.03]	[10.38–21.83]	[7.29–24.66]	$\mathcal{N}(12, 4)$
$\gamma_{COR07(DRS-3.4)}$	($m\,s^{-1}$)	4281.50	4281.91	4282.18	2.27	4282.11	[4279.94–4284.45]	[4277.87–4286.97]	[4275.82–4289.55]	$\mathcal{U}$
					Noise					
$\sigma_{COR98(DRS-3.3)}$	($m\,s^{-1}$)	8.66	8.89	9.87	2.82	9.46	[7.25–12.47]	[5.51–16.73]	[4.17–23.36]	$\mathcal{U}$
$\sigma_{COR14(DRS-3.8)}$	($m\,s^{-1}$)	0.62	0.46	1.75	1.29	1.51	[0.47–3.00]	[0.07–4.90]	[0.00–7.73]	$\mathcal{U}$
$\sigma_{COR07(DRS-3.4)}$	($m\,s^{-1}$)	5.63	6.49	6.73	1.15	6.64	[5.61–7.85]	[4.73–9.32]	[3.95–11.07]	$\mathcal{U}$
					HD 98649b					
$\log P$	(d)	3.7508	3.7808	3.7848	0.0240	3.7834	[3.7611–3.8086]	[3.7409–3.8373]	[3.7222–3.8692]	$\mathcal{U}$
$\log K$	($m\,s^{-1}$)	2.1918	2.1458	2.1817	0.0622	2.1650	[2.1272–2.2386]	[2.1061–2.3537]	[2.0906–2.4329]	$\mathcal{U}$
$\sqrt{e}\cos\omega$		−0.3301	−0.2764	−0.3155	0.0796	−0.2974	[−0.3900–0.2445]	[−0.5267–0.2028]	[−0.5957–0.1629]	$\mathcal{U}$
$\sqrt{e}\sin\omega$		−0.8689	−0.8808	−0.8715	0.0221	−0.8769	[−0.8885–0.8572]	[−0.8984–0.8016]	[−0.9072–0.7610]	$\mathcal{U}$
T_{Vmax}	(BJD)	2455271.6	2455264.7	2455262.2	14.1	2455263.5	[2455250.4–2455274.8]	[2455227.6–2455286.4]	[2455190.8–2455299.0]	$\mathcal{U}$
a_S	(AU)	0.04055	0.04129	0.04223	0.00280	0.04178	[0.03969–0.04477]	[0.03789–0.04939]	[0.03626–0.05465]	–
a	(AU)	6.097	6.570	6.609	0.277	6.594	[6.336–6.881]	[6.105–7.212]	[5.891–7.586]	–
e		0.8640	0.8556	0.8659	0.0253	0.8626	[0.8410–0.8927]	[0.8239–0.9223]	[0.8087–0.9403]	–
K	($m\,s^{-1}$)	155.5	140.1	153.6	24.4	146.2	[134.0–173.2]	[127.7–225.8]	[123.2–270.9]	–
ω	(°)	249.20	252.61	250.16	4.99	251.29	[245.58–254.58]	[236.70–257.20]	[231.95–259.71]	–
m	($M_\oplus$)	2101	2157	2194	148	2175	[2059–2325]	[1954–2574]	[1856–2829]	–
m	(M_J)	6.610	6.788	6.905	0.466	6.843	[6.479–7.315]	[6.148–8.098]	[5.839–8.903]	–
m	($M_\odot$)	0.006309	0.006479	0.006591	0.000445	0.006532	[0.006184–0.006982]	[0.005868–0.007729]	[0.005574–0.008498]	–
P	(d)	5633	6024	6103	341	6073	[5769–6436]	[5506–6875]	[5274–7399]	–
T_C	(BJD)	2454102	2453718	2453924	410	2453860	[2453525–2454369]	[2453243–2454828]	[2452944–2454969]	–
T_P	(BJD)	2455128.3	2455121.7	2455116.0	22.1	2455117.9	[2455093.6–2455138.5]	[2455066.9–2455153.8]	[2455042.6–2455164.4]	–

Notes. The maximum likelihood solution, median, mode, and standard-deviation of the posterior distribution for each parameter are shown, as well as the 68.27, 95.45, and 99.73% confidence intervals. The prior for each parameter can be of type: $\mathcal{U}$: uniform, $\mathcal{N}$: normal, or $\mathcal{TN}$: truncated normal. Reference epoch: 2455500.0 BJD.

Table B.6. Parameters probed by the MCMC used to fit the RV measurements of HD 50499.

Parameter	Units	Max(Likelihood)	Mode	Mean	Std	Median	68.27%	95.45%	99.73%	Prior
log(Likelihood)		−668.22	−677.90	−678.84	3.49	−678.50	[−682.24–675.41]	[−686.79–672.90]	[−692.68–671.11]	–
					Star					
M_S	($M_\odot$)	1.3739	1.3102	1.3098	0.0699	1.3102	[1.2402–1.3795]	[1.1687–1.4483]	[1.0980–1.5220]	$\mathcal{U}$
Π_S	(mas)	99.91	100.03	99.99	1.00	100.00	[98.98–100.99]	[97.99–101.98]	[96.91–103.08]	$\mathcal{U}$
					Offset					
$\gamma_{\rm HIRES(Pub-2017)}$	($m\,s^{-1}$)	−36798.27	−36798.15	−36798.23	1.45	−36798.21	[−36799.68–36796.79]	[−36801.16–36795.38]	[−36802.59–36794.00]	$\mathcal{U}$
$\gamma_{\rm COR98(DRS-3.3)}$	($m\,s^{-1}$)	3.63	3.77	3.71	1.95	3.72	[1.76–5.68]	[−0.21–7.57]	[−2.15–9.55]	$\mathcal{N}(0,4)$
$\gamma_{\rm COR07(DRS-3.4)}$	($m\,s^{-1}$)	36813.30	36814.53	36817.23	6.52	36815.30	[36812.73–36821.25]	[36810.66–36838.24]	[36808.80–36850.47]	$\mathcal{U}$
$\gamma_{\rm HARPS03(DRS-3.5)}$	($m\,s^{-1}$)	32.74	31.73	31.76	2.32	31.75	[29.47–34.04]	[27.06–36.43]	[24.66–39.01]	$\mathcal{N}(32,4)$
$\gamma_{\rm COR14(DRS-3.8)}$	($m\,s^{-1}$)	17.56	16.71	16.80	2.60	16.78	[14.25–19.38]	[11.59–22.11]	[8.46–24.74]	$\mathcal{N}(12,4)$
					Noise					
$\sigma_{\rm HIRES(Pub-2017)}$	($m\,s^{-1}$)	3.956	4.178	4.247	0.410	4.220	[3.838–4.658]	[3.503–5.139]	[3.212–5.777]	$\mathcal{U}$
$\sigma_{\rm COR98(DRS-3.3)}$	($m\,s^{-1}$)	7.34	7.71	7.95	1.16	7.85	[6.81–9.09]	[5.93–10.53]	[5.12–12.29]	$\mathcal{U}$
$\sigma_{\rm COR07(DRS-3.4)}$	($m\,s^{-1}$)	7.42	7.52	7.84	1.22	7.73	[6.65–9.03]	[5.73–10.58]	[4.94–12.62]	$\mathcal{U}$
$\sigma_{\rm HARPS03(DRS-3.5)}$	($m\,s^{-1}$)	1.81	2.24	3.20	2.11	2.68	[1.71–4.49]	[1.12–8.72]	[0.67–18.95]	$\mathcal{U}$
$\sigma_{\rm COR14(DRS-3.8)}$	($m\,s^{-1}$)	4.79	5.04	5.19	1.02	5.12	[4.19–6.19]	[3.36–7.42]	[2.56–8.91]	$\mathcal{U}$
					HD 50499b					
$\log P$	(d)	3.39372	3.39533	3.39536	0.00333	3.39535	[3.39207–3.39867]	[3.38870–3.40205]	[3.38489–3.40537]	$\mathcal{U}$
$\log K$	($m\,s^{-1}$)	1.2733	1.2783	1.2766	0.0195	1.2772	[1.2573–1.2959]	[1.2361–1.3150]	[1.2148–1.3338]	$\mathcal{U}$
$\sqrt{e}\cos\omega$		−0.1092	−0.1029	−0.1038	0.0773	−0.1033	[−0.1813–0.0262]	[−0.2583–0.0484]	[−0.3288–0.1272]	$\mathcal{U}$
$\sqrt{e}\sin\omega$		−0.5199	−0.5129	−0.5060	0.0458	−0.5082	[−0.5507–0.4615]	[−0.5915–0.4069]	[−0.6298–0.3356]	$\mathcal{U}$
$T_{\rm Vmin}$	(BJD)	2455823.0	2455820.7	2455825.2	33.8	2455823.4	[2455791.7–2455858.5]	[2455762.5–2455898.4]	[2455733.0–2455940.5]	$\mathcal{U}$
a_S	(AU)	0.004096	0.004160	0.004153	0.000184	0.004154	[0.003971–0.004336]	[0.003784–0.004523]	[0.003595–0.004701]	–
a	(AU)	3.9830	3.9293	3.9288	0.0730	3.9298	[3.8567–4.0018]	[3.7783–4.0719]	[3.6983–4.1391]	–
e		0.2822	0.2725	0.2749	0.0382	0.2739	[0.2376–0.3124]	[0.2004–0.3549]	[0.1642–0.4003]	–
K	($m\,s^{-1}$)	18.763	18.944	18.927	0.850	18.930	[18.083–19.767]	[17.223–20.653]	[16.399–21.568]	–
ω	(°)	258.14	259.32	258.18	9.08	258.55	[249.13–267.21]	[238.96–275.11]	[227.46–283.12]	–
m	($M_\oplus$)	470.6	460.6	460.8	25.6	460.7	[435.4–486.4]	[410.1–512.8]	[385.2–540.9]	–
m	(M_J)	1.4809	1.4494	1.4501	0.0807	1.4497	[1.3699–1.5304]	[1.2905–1.6136]	[1.2121–1.7021]	–
m	($M_\odot$)	0.0014135	0.0013834	0.0013841	0.0000770	0.0013837	[0.0013076–0.0014608]	[0.0012318–0.0015402]	[0.0011569–0.0016247]	–
P	(d)	2475.8	2484.6	2485.3	19.1	2485.1	[2466.5–2504.2]	[2447.4–2523.8]	[2426.0–2543.1]	–
T_C	(BJD)	2455055.5	2455060.8	2455055.6	50.9	2455057.1	[2455004.9–2455106.4]	[2454950.1–2455153.9]	[2454889.1–2455194.6]	–
T_P	(BJD)	2457073.4	2456172.9	2456164.6	58.8	2456167.7	[2456105.4–2456223.3]	[2456040.3–2456273.6]	[2455966.5–2456322.7]	–
					HD 50499c					
$\log P$	(d)	3.9217	3.9390	3.9819	0.0949	3.9509	[3.9140–4.0506]	[3.8848–4.2905]	[3.8590–4.4037]	$\mathcal{U}$
$\log K$	($m\,s^{-1}$)	1.3722	1.3816	1.4081	0.0555	1.3917	[1.3670–1.4475]	[1.3473–1.5814]	[1.3297–1.6610]	$\mathcal{U}$
$\sqrt{e}\cos\omega$		0.086	−0.058	−0.103	0.220	−0.089	[−0.344–0.132]	[−0.549–0.279]	[−0.642–0.401]	$\mathcal{U}$
$\sqrt{e}\sin\omega$		0.197	0.099	0.080	0.117	0.085	[−0.046–0.204]	[−0.159–0.286]	[−0.256–0.349]	$\mathcal{U}$
$T_{\rm Vmin}$	(BJD)	2454510.8	2454559.9	2454549.0	73.8	2454551.4	[2454475.4–2454621.0]	[2454394.8–2454692.6]	[2454316.7–2454770.4]	$\mathcal{U}$
a_S	(AU)	0.0181	0.0191	0.0240	0.0115	0.0201	[0.0177–0.0286]	[0.0161–0.0634]	[0.0148–0.0970]	–
a	(AU)	8.96	9.02	9.78	1.68	9.24	[8.69–10.75]	[8.27–15.51]	[7.88–18.57]	–
e		0.0460	0.0000	0.0792	0.0761	0.0571	[0.0171–0.1365]	[0.0026–0.3079]	[0.0002–0.4259]	–
K	($m\,s^{-1}$)	23.56	24.23	25.82	3.78	24.64	[23.28–28.02]	[22.25–38.14]	[21.37–45.82]	–
ω	(°)	66	180	50	113	81	[−115–161]	[−177–177]	[−180–180]	–
m	($M_\oplus$)	923	932	1032	239	957	[874–1164]	[814–1801]	[759–2346]	–
m	(M_J)	2.904	2.932	3.246	0.751	3.011	[2.752–3.664]	[2.560–5.666]	[2.387–p7.382]	–
m	($M_\odot$)	0.002772	0.002799	0.003098	0.000717	0.002874	[0.002626–0.003497]	[0.002444–0.005408]	[0.002278–0.007046]	–
P	(d)	8350	8611	9861	2745	8932	[8204–11235]	[7671–19522]	[7228–25332]	–
T_C	(BJD)	2456009	2461130	2462211	2525	2461357	[2460705–2463463]	[2460175–2471070]	[2459652–2476577]	–
T_P	(BJD)	2455509	2461832	2462479	4026	2461969	[2458947–2465593]	[2456054–2474140]	[2455527–2479915]	–

Notes. The maximum likelihood solution, median, mode, and standard-deviation of the posterior distribution for each parameter are shown, as well as the 68.27%, 95.45%, and 99.73% confidence intervals. The prior for each parameter can be of type: $\mathcal{U}$: uniform, $\mathcal{N}$: normal, or $\mathcal{TN}$: truncated normal. Reference epoch: 2455500.0 BJD.

Table B.7. Parameters probed by the MCMC used to fit the RV measurements of HD 92788.

Parameter	Units	Max(Likelihood)	Mode	Mean	Std	Median	68.27%	95.45%	99.73%	Prior
log(Likelihood)		−625.86	−636.46	−637.60	3.58	−637.24	[−641.13–634.06]	[−645.81–631.54]	[−650.84–629.55]	–
Star										
M_S	($M_\odot$)	1.1684	1.1483	1.1500	0.0702	1.1500	[1.0805–1.2202]	[1.0089–1.2907]	[0.9272–1.3575]	$\mathcal{U}$
Π_S	(mas)	28.838	28.835	28.829	0.288	28.828	[28.541–29.120]	[28.254–29.406]	[27.958–29.662]	$\mathcal{U}$
Offset										
$\gamma_{\rm COR14(DRS-3.8)}$	($m\,s^{-1}$)	9.64	10.96	10.84	3.53	10.83	[7.32–14.39]	[3.89–17.94]	[0.33–21.77]	$\mathcal{N}(12,4)$
$\gamma_{\rm COR07(DRS-3.4)}$	($m\,s^{-1}$)	−4430.37	−4430.03	−4430.76	2.76	−4430.42	[−4433.39–4428.15]	[−4437.43–4426.17]	[−4440.86–4423.54]	$\mathcal{U}$
$\gamma_{\rm HAMILTON(Pub-2006)}$	($m\,s^{-1}$)	4448.46	4448.30	4448.04	2.68	4448.10	[4445.39–4450.72]	[4442.43–4453.25]	[4439.52–4455.84]	$\mathcal{U}$
$\gamma_{\rm COR98(DRS-3.3)}$	($m\,s^{-1}$)	−1.95	−2.24	−2.24	2.29	-2.21	[−4.51–0.03]	[−6.94–2.25]	[−9.77–4.46]	$\mathcal{N}(0,4)$
$\gamma_{\rm HARPS03(DRS-3.5)}$	($m\,s^{-1}$)	38.84	38.53	38.23	1.84	38.33	[36.45–40.02]	[34.19–41.68]	[31.45–43.36]	$\mathcal{N}(32,4)$
$\gamma_{\rm HIRES(Pub-2017)}$	($m\,s^{-1}$)	4470.60	4470.24	4470.10	1.93	4470.16	[4468.25–4472.01]	[4465.96–4473.73]	[4462.84–4475.55]	$\mathcal{U}$
Noise										
$\sigma_{\rm COR07(DRS-3.4)}$	($m\,s^{-1}$)	2.42	3.96	4.54	2.72	4.24	[1.90–6.99]	[0.33–10.98]	[0.02–17.75]	$\mathcal{U}$
$\sigma_{\rm HIRES(Pub-2017)}$	($m\,s^{-1}$)	3.521	3.752	3.831	0.531	3.788	[3.311–4.355]	[2.911–5.025]	[2.576–5.898]	$\mathcal{U}$
$\sigma_{\rm COR14(DRS-3.8)}$	($m\,s^{-1}$)	2.91	4.08	4.60	2.14	4.36	[2.65–6.52]	[0.96–9.71]	[0.07–14.94]	$\mathcal{U}$
$\sigma_{\rm HAMILTON(Pub-2006)}$	($m\,s^{-1}$)	4.85	5.16	5.08	2.22	5.09	[2.82–7.25]	[0.62–9.64]	[0.03–12.51]	$\mathcal{U}$
$\sigma_{\rm COR98(DRS-3.3)}$	($m\,s^{-1}$)	9.36	9.58	9.83	1.35	9.75	[8.49–11.17]	[7.40–12.78]	[6.42–14.65]	$\mathcal{U}$
$\sigma_{\rm HARPS03(DRS-3.5)}$	($m\,s^{-1}$)	1.431	1.491	1.535	0.194	1.523	[1.344–1.727]	[1.186–1.960]	[1.045–2.215]	$\mathcal{U}$
HD 92788b										
$\log P$	(d)	2.5128215	2.5128306	2.5128344	0.0000622	2.5128330	[2.5127722–2.5128955]	[2.5127131–2.5129638]	[2.5126589–2.5130376]	$\mathcal{U}$
$\log K$	($m\,s^{-1}$)	2.03396	2.03454	2.03446	0.00351	2.03447	[2.03100–2.03795]	[2.02741–2.04146]	[2.02355–2.04503]	$\mathcal{U}$
$\sqrt{e}\cos\omega$		0.0809	0.0797	0.0800	0.0113	0.0800	[0.0687–0.0912]	[0.0573–0.1026]	[0.0452–0.1144]	$\mathcal{U}$
$\sqrt{e}\sin\omega$		−0.58785	−0.58698	−0.58697	0.00398	−0.58699	[−0.59092–0.58302]	[−0.59485–0.57895]	[−0.59886–0.57446]	$\mathcal{U}$
λ_0	(°)	115.191	115.166	115.125	0.474	115.140	[114.656–115.591]	[114.128–116.041]	[113.540–116.525]	$\mathcal{U}$
a_S	(AU)	0.0030300	0.0030350	0.0030349	0.0000271	0.0030348	[0.0030080–0.0030619]	[0.0029814–0.0030896]	[0.0029521–0.0031194]	–
a	(AU)	0.9768	0.9720	0.9712	0.0198	0.9716	[0.9517–0.9910]	[0.9302–1.0097]	[0.9044–1.0267]	–
e		0.35211	0.35120	0.35108	0.00451	0.35108	[0.34660–0.35558]	[0.34200–0.36013]	[0.33750–0.36478]	–
K	($m\,s^{-1}$)	108.133	108.243	108.262	0.874	108.261	[107.400–109.131]	[106.516–110.016]	[105.571–110.926]	–
ω	(°)	−82.17	−82.27	−82.24	1.10	−82.24	[−83.33–81.16]	[−84.44–80.04]	[−85.61–78.90]	–
m	($M_\oplus$)	1208.0	1195.9	1196.7	50.0	1196.9	[1147.2–1247.0]	[1095.5–1295.0]	[1037.4–1343.4]	–
m	(M_J)	3.801	3.763	3.766	0.157	3.766	[3.610–3.924]	[3.447–4.075]	[3.264–4.227]	–
m	($M_\odot$)	0.003628	0.003592	0.003594	0.000150	0.003595	[0.003446–0.003745]	[0.003290–0.003890]	[0.003116–0.004035]	–
P	(d)	325.7028	325.7097	325.7125	0.0467	325.7114	[325.6659–325.7583]	[325.6215–325.8095]	[325.5809–325.8649]	–
T_C	(BJD)	2455470.50	2455470.61	2455470.65	1.29	2455470.64	[2455469.38–2455471.93]	[2455468.11–2455473.28]	[2455466.78–2455474.73]	–
T_P	(BJD)	2455543.031	2455647.141	2455647.142	0.736	2455647.139	[2455646.415–2455647.868]	[2455645.674–2455648.640]	[2455644.949–2455649.443]	–
HD 92788c										
$\log P$	(d)	4.077	4.065	4.122	0.107	4.094	[4.030–4.222]	[3.984–4.410]	[3.945–4.597]	$\mathcal{U}$
$\log K$	($m\,s^{-1}$)	1.5369	1.5238	1.5239	0.0278	1.5239	[1.4962–1.5517]	[1.4684–1.5805]	[1.4393–1.6035]	$\mathcal{U}$
$\sqrt{e}\cos\omega$		0.6302	0.6139	0.6196	0.0554	0.6185	[0.5676–0.6730]	[0.5065–0.7354]	[0.4308–0.7870]	$\mathcal{U}$
$\sqrt{e}\sin\omega$		−0.2734	−0.3134	−0.3152	0.0947	−0.3135	[-0.4112–0.2213]	[−0.5121–0.1313]	[−0.5867–0.0255]	$\mathcal{U}$
$T_{\rm Vmax}$	(BJD)	2457168.9	2457142.6	2457122.4	99.5	2457129.7	[2457025.2–2457220.2]	[2456899.1–2457298.5]	[2456754.7–2457390.4]	$\mathcal{U}$
a_S	[AU]	0.03328	0.03195	0.03578	0.00782	0.03359	[0.02964–0.04200]	[0.02686–0.05768]	[0.02452–0.08454]	–
a	(AU)	10.77	10.50	11.65	2.18	11.00	[9.95–13.40]	[9.24–17.84]	[8.65–23.92]	–
e		0.4719	0.4551	0.4952	0.0767	0.4793	[0.4241–0.5739]	[0.3805–0.6820]	[0.3427–0.7579]	–
K	($m\,s^{-1}$)	34.43	33.29	33.48	2.14	33.41	[31.35–35.62]	[29.40–38.06]	[27.50–40.13]	–
ω	(°)	−23.45	−25.71	−26.79	7.89	−26.49	[−34.63–19.08]	[−43.21–11.50]	[−52.07–2.23]	–
m	($M_\oplus$)	1203.2	1164.8	1172.1	87.7	1169.0	[1084.5–1260.1]	[1004.8–1356.5]	[929.2–1455.6]	–
m	(M_J)	3.786	3.665	3.688	0.276	3.678	[3.413–3.965]	[3.162–4.268]	[2.924–4.580]	–
m	($M_\odot$)	0.003614	0.003498	0.003520	0.000264	0.003511	[0.003257–0.003785]	[0.003018–0.004074]	[0.002791–0.004372]	–
P	(d)	11927	11610	13703	4106	12405	[10706–16666]	[9639–25718]	[8804–39575]	–
T_C	(BJD)	2461454	2458838	2458997	386	2458921	[2458666–2459320]	[2458452–2460040]	[2458240–2460932]	–
T_P	(BJD)	2456919	2456858	2456825	167	2456834	[2456656–2456991]	[2456473–2457133]	[2456281–2457257]	–

Notes. The maximum likelihood solution, median, mode, and standard-deviation of the posterior distribution for each parameter are shown, as well as the 68.27, 95.45, and 99.73% confidence intervals. The prior for each parameter can be of type: $\mathcal{U}$: uniform, $\mathcal{N}$: normal, or $\mathcal{TN}$: truncated normal. Reference epoch: 2455500.0 BJD.